

1 **An assessment of geographical distribution of different plant functional types**
2 **over North America simulated using the CLASS-CTEM modelling**
3 **framework**

4

5 **Rudra K. Shrestha¹, Vivek K. Arora¹, Joe R. Melton², and Laxmi Sushama³**

6 ¹Canadian Centre for Climate Modelling and Analysis, Environment and Climate Change Canada,
7 University of Victoria, Victoria, BC, V8W 2Y2, Canada

8 ²Climate Research Division, Environment and Climate Change Canada, Toronto, Ontario, Canada

9 ³Département des sciences de la Terre et de l'atmosphère, Université du Québec à Montréal, Canada

10

11 *Correspondence to: V. K. Arora (Vivek.Arora@canada.ca)*

12

13 **Abstract**

14

15 The performance of the competition module of the CLASS-CTEM (Canadian Land Surface
16 Scheme and Canadian Terrestrial Ecosystem Model) modelling framework is assessed at 1°
17 spatial resolution over North America by comparing the simulated geographical distribution of
18 its plant functional types (PFTs) with two observation-based estimates. The model successfully
19 reproduces the broad geographical distribution of trees, grasses and bare ground although
20 limitations remain. In particular, compared to the two observation-based estimates, the simulated
21 fractional vegetation coverage is lower in the arid south-west North American region and higher
22 in the Arctic region. The lower than observed simulated vegetation coverage in the south-west
23 region is attributed to lack of representation of shrubs in the model and plausible errors in the
24 observation-based data sets. The observation-based data indicates vegetation fractional coverage
25 of more than 60% in this arid region, despite only 200-300 mm of precipitation that the region
26 receives annually and observation-based leaf area index (LAI) values in the region are lower than
27 one. The higher than observed vegetation fractional coverage in the Arctic is likely due to the
28 lack of representation of moss and lichen PFTs and also likely because of inadequate
29 representation of permafrost in the model as a result of which the C₃ grass PFT performs overly
30 well in the region. The model generally reproduces the broad spatial distribution and the total
31 area covered by the two primary tree PFTs (needleleaf evergreen and broadleaf cold deciduous

32 trees) reasonably well. The simulated fractional coverage of tree PFTs increases after 1960s in
33 response to the CO₂ fertilization effect and climate warming. Differences between observed and
34 simulated PFT coverages highlight model limitations ~~and suggest that the inclusion of shrubs,~~
35 ~~and moss and lichen PFTs, and an adequate representation of permafrost will help improve~~
36 ~~model performance.~~

Deleted: in the model

Deleted: and

Deleted: provide insight into physical and structural processes that need improvement

37

38

44 1 Introduction

45

46 The terrestrial ecosystem plays an important role in regulating climate and weather through land-
47 atmosphere exchange of water and energy (Cramer et al., 2001; Garraud et al., 2015; Pielke et
48 al., 1998; Ran et al., 2016) and in mitigating climate change by sequestering atmospheric CO₂
49 (Bonan, 2008; Timmons et al., 2016). The projected sink of atmospheric CO₂ is uncertain due to
50 disagreements among the Earth system models (ESMs) (Arora et al., 2013; Friedlingstein et al.,
51 2006) primarily due to differing responses of their terrestrial ecosystem modules to future
52 changes in atmospheric CO₂. This uncertainty arises primarily because of the differences in the
53 strength of the CO₂ fertilization effect on the land carbon cycle components (Arora et al., 2013;
54 Cramer et al., 2001; Friend et al., 2013) but also because of differences in the response of
55 vegetation. Models differ in how the spatial distribution of vegetation, and its composition,
56 changes in response to changing climate and increasing CO₂ (Cramer et al., 2001). These
57 differences are also resolution dependent. For example, models with coarse grid resolutions
58 cannot explicitly resolve climatic niches, which in turn potentially contributes to biases in
59 simulated vegetation distribution (Melton and Arora, 2016; Shrestha et al., 2016).

60

61 Vegetation responds to changes in climate and atmospheric CO₂ concentration by changing its
62 structural attributes including leaf area index (LAI), rooting depth, vegetation height, and canopy
63 mass, as well as its areal extent. Structural vegetation changes generally occur over seasonal to
64 decadal time scales (Kramer and Kozlowski, 1979), while the slower areal extent changes
65 typically occur on decadal to centennial time scales (Ritchie and Macdonald, 1986). The
66 dynamic behavior of vegetation affects weather and climate due to its strong control over
67 biophysical processes. At hourly to daily timescales, vegetation affects the exchange of water
68 and energy between the land surface and the atmosphere primarily through the control of leaf
69 stomata. At longer ~~seasonal, annual and decadal~~ timescales, vegetation affects components of
70 energy and water balance through its structure (LAI, rooting depth, etc.) and its areal extent and
71 thereby land surface albedo. Conversely, dynamics of vegetation is directly influenced by
72 climate and the competitive ability of the plants. In this way vegetation responds to climate by
73 changing its structure and areal extent depending on the colonization ability of plants. These

Deleted: timescales from

Deleted: to

76 climate-vegetation interactions have been well documented (e.g. Gobron et al., 2010; Wang et
77 al., 2011).

78
79 Natural vegetation is typically characterized in dynamic global vegetation models (DGVMs)
80 based on a limited number of PFTs (Sitch et al., 2003) because it is impossible to represent
81 thousands of species in a model. Species characterized by similar attributes, mainly based on
82 their form and interactions with the environment (Box, 1996), are grouped together as a single
83 PFT. For example, tree species with similar leaf form such as fir (*Abies*), spruce (*Picea*) and pine
84 (*Pinus*) are classified as needleleaf evergreen trees. The geographical distribution of the PFTs in
85 DGVMs is determined by their ability to grow and increase their areal extent given certain
86 climate and soil conditions and their competitive ability.

87
88 One way of representing competition between PFTs in DGVMs is through the use of the Lotka-
89 Volterra (LV) equations. While originally developed for predator-prey competition, the LV
90 equations have been used in a number of DGVMs (Arora and Boer, 2006; Brentnall et al., 2005;
91 Cox, 2001; Zhang et al., 2015). The use of the classical form of the LV equations for modelling
92 competition between PFTs, however, leads to an amplified expression of dominance in that the
93 dominant PFT ends up occupying a disproportionately large fraction of a grid cell leading to
94 little co-existence between PFTs. Arora and Boer (2006) proposed changes to the classical
95 implementation of the LV equations for modelling competition between PFTs to reduce this
96 amplified expression of dominance. Their approach, which has been implemented in the CLASS-
97 CTEM modelling framework and which allows improved co-existence of PFTs compared to the
98 classical LV equations, has been shown to simulate vegetation distribution reasonably well at the
99 global (Melton and Arora, 2016) as well as point (Shrestha et al., 2016) scales. Both these
100 studies used climate averaged over $\sim 3.75^\circ$ spatial resolution. The CLASS-CTEM framework
101 consists of the Canadian Land Surface Scheme (CLASS) coupled to the Canadian Terrestrial
102 Ecosystem Model (CTEM) which is a dynamic vegetation model.

103
104 In this paper, we evaluate the competition module of the CLASS-CTEM modelling framework at
105 the regional scale over the North American domain at 1° spatial resolution. This resolution is
106 much finer than the 3.75° resolution used in the Melton and Arora (2016) study and therefore in

Deleted:

108 principle should allow a more realistic simulation of geographical distribution of PFTs as climate
109 niches are resolved.

110
111 The rest of this paper is organized as follows: Section 2 describes the CLASS-CTEM modelling
112 framework, details of the observation-based data and the experimental setup. Results are
113 presented in section 3 and a discussion follows in section 4. Finally, a summary and conclusions
114 are provided in section 5.

115

116 | **2 Model, data and methods**

Deleted:

117

118 | **2.1 CLASS-CTEM model**

119

120 The results presented here are obtained by coupling version 2.0 of CTEM (Melton and Arora,
121 2016), which dynamically simulates fractional coverage of its PFTs, to version 3.6 of CLASS
122 (Verseghy et al., 1993). CTEM simulates terrestrial processes for seven non-crop and two crop
123 PFTs (Table 1) and prognostically tracks carbon in three living vegetation components (leaves,
124 stems and roots) and two dead carbon pools (litter and soil). The terrestrial ecosystem processes
125 simulated in this study include photosynthesis, autotrophic respiration, heterotrophic respiration,
126 dynamic leaf phenology, allocation of carbon from leaves to stem and root components, fire,
127 land use change, and competition between PFTs which dynamically determines the fractional
128 coverage of each PFT. The amount of carbon in the leaf, stem and root components is used to
129 estimate structural attributes of vegetation. LAI is calculated from leaf biomass using PFT-
130 dependent specific leaf area (SLA) which determines area of leaves that can be constructed per
131 kg C of leaf biomass (Arora and Boer, 2005); vegetation height is calculated based on stem
132 biomass for tree PFTs and LAI for grass PFTs; and rooting depth is calculated based on root
133 biomass (Arora and Boer, 2003). CTEM operates at a time step of one day except for
134 photosynthesis and leaf respiration which are calculated every 30 minutes for consistency with
135 CLASS' energy and water balance calculations which require stomatal resistance calculated by
136 the photosynthesis module of CTEM.

137

139 CLASS simulates the energy and water balance components at the land surface and operates at a
 140 30 minutes time step. Liquid and frozen soil moisture and soil temperature are evaluated for
 141 three soil layers (with maximum thicknesses of 0.1, 0.25 and 3.75 m). The actual thicknesses of
 142 these permeable soil layers are determined by the depth to bedrock, which is specified on the
 143 basis of the global data set of Zobler (1986). CLASS distinguishes four PFTs (needleleaf trees,
 144 broadleaf trees, crops and grasses) which map directly to the nine PFTs represented in CTEM as
 145 shown in Table 1. Needleleaf trees in CTEM are divided into deciduous and evergreen types,
 146 broadleaf trees are divided into cold and drought deciduous and evergreen types, and crops and
 147 grasses are divided into C₃ and C₄ types based on their photosynthetic pathways. In coupled
 148 mode, CLASS uses the dynamically simulated vegetation attributes (including LAI, vegetation
 149 height, canopy mass and rooting depth) and stomatal resistance calculated by CTEM, and CTEM
 150 uses the soil moisture, soil temperature and net shortwave radiation calculated by CLASS. The
 151 coupling frequency between CLASS and CTEM is one day.

152

153 2.1.1 Competition parameterization

154

155 Competition between PFTs in CTEM is parameterized following Arora and Boer (2006) who
 156 presented a modified version of the LV equations. The approach is described in detail by Melton
 157 and Arora (2016) and briefly summarized here. Consider, for simplicity, two PFTs that exist in a
 158 grid cell with fractional coverages f_1 and f_2 . Let PFT 1 represent a tree PFT and PFT 2 represent
 159 a grass PFT. The bare fraction of grid cell not covered by any vegetation is represented by f_B . As
 160 a result, $f_1 + f_2 + f_B = 1$. The rate of change of fractional coverages of the two PFTs and bare
 161 fraction, for this example, are given by,

162

$$163 \left| \frac{df_1}{dt} = c_1 f_1^\beta (1 - f_1) - m_1 f_1 \right. \quad (1)$$

164

$$165 \left| \frac{df_2}{dt} = c_2 f_2^\beta (1 - f_1 - f_2) - c_1 f_1^\beta f_2 - m_2 f_2 \right. \quad (2)$$

166

$$167 \left| \frac{df_B}{dt} = -c_1 f_1^\beta f_B - c_2 f_2^\beta f_B + m_1 f_1 + m_2 f_2 \right. \quad (3)$$

168

169 where c_1 , c_2 and m_1 , m_2 are the colonization and mortality rates for PFT 1 and PFT 2,
170 respectively. Colonization and mortality rates cannot be negative. Equations (1) and (2) show
171 that PFT 1 can invade the fraction covered by PFT 2 and the bare fraction; and that PFT 2 can
172 only invade the bare fraction. PFT 2 is not allowed to invade the fraction covered by PFT 1
173 because it is ranked lower than PFT 1. In CTEM, the superiority or ranking of the seven natural
174 non-crop PFTs is based on the tree-grass distinction and their colonization rates. Trees are always
175 considered to be superior than grasses because of their ability to shade them (Siemann and
176 Rogers, 2003). Within the tree and grass PFTs the dominance is determined dynamically based
177 on the colonization rate. The exponent β ($0 \leq \beta \leq 1$), an empirical parameter, controls the
178 behaviour of the LV equations. For $\beta = 1$, the equations represent the classical form of the LV
179 equations. The equilibrium fractional coverages for PFT 1 and 2 and bare fraction for this
180 classical form of the LV equations, denoted by \tilde{f}_1, \tilde{f}_2 and are given by,

$$\tilde{f}_1 = \max\left\{\left(\frac{c_1 - m_1}{c_1}\right), 0\right\} \quad (4)$$

$$\tilde{f}_2 = \max\left\{\left(\frac{(c_2 - m_2) - \left(1 + \frac{c_2}{c_1}\right)(c_1 - m_1)}{c_2}\right), 0\right\} \quad (5)$$

$$\tilde{f}_B = \frac{(m_1 \tilde{f}_1 + m_2 \tilde{f}_2)}{(c_1 \tilde{f}_1 + c_2 \tilde{f}_2)} \quad (6)$$

188 In equations (1) and (2), if the fractional coverages of PFT 1 and PFT 2 are initially zero then the
189 PFTs cannot expand for $\beta = 1$, implying that a minimum seeding fraction is always required.
190 Furthermore, in equation (5) as long as $(c_1 - m_1)$ is greater than $(c_2 - m_2)$ then the equilibrium
191 solution for \tilde{f}_2 will always be zero and PFT 2 will not be able to coexist with PFT 1. These
192 features of the classical form of the LV equations are avoided when $\beta = 0$, following Arora and
193 Boer (2006). The equilibrium fractional coverages for PFT 1 and 2 and bare fraction for the case
194 with $\beta = 0$ are given by,

$$\tilde{f}_1 = \left(\frac{c_1}{c_1 + m_1}\right) \quad (7)$$

$$\tilde{f}_2 = \frac{c_2(1 - \tilde{f}_1)}{(c_1 + c_2 + m_2)} = \left(\frac{c_2 m_1}{(c_1 + m_1)(c_1 + c_2 + m_2)}\right) \quad (8)$$

198
$$\tilde{f}_B = \frac{(m_1 \tilde{f}_1 + m_2 \tilde{f}_2)}{(c_1 + c_2)} \quad (9)$$

199 Unlike the classical version of the LV equations, the modified version of the equations with $\beta = 0$
 200 does not require a minimum seeding fraction, and PFTs are able to increase their areal extent as
 201 long as the climate is favorable and c_i is positive. Also, as long as $m_1 > 0$ and $c_2 > 0$ then PFT 2
 202 is able to coexist at equilibrium with PFT 1. Other values of β between 0 and 1 give the dominant
 203 PFT varying levels of access to sub-dominant PFTs but coexistence is most possible in the case
 204 with $\beta = 0$.

205
 206 The calculations of colonization and mortality rates are described in detail in Melton and Arora
 207 (2016). Briefly, the colonization rate depends on the net primary productivity of a PFT. The
 208 better a PFT performs for given climatic and soil conditions; the higher is its colonization rate.
 209 The mortality rate represents the combined effect of four different processes: intrinsic or age-
 210 related mortality, growth or stress mortality, mortality due to disturbance, and mortality due to
 211 adverse climate which ensures that tree PFTs do not venture outside their bioclimatic zones.

212
 213 **2.2 Forcing data**

214
 215 The Climate Research Unit – National Centre for Environmental Prediction (CRU-NCEP)
 216 reanalysis dataset (Viovy, 2012), is used to drive the model. The meteorological variables
 217 (surface temperature, pressure, precipitation, wind, specific humidity, and incident short-wave
 218 and long-wave radiation fluxes) are available at a spatial resolution of $0.5^\circ \times 0.5^\circ$ and at a six
 219 hourly time interval for the period 1901-2010. These data are interpolated to 1° resolution
 220 spatially, and disaggregated to half-hourly time resolution, a standard CLASS-CTEM model
 221 integration time step. Temperature, pressure, wind, specific humidity, and long-wave radiation
 222 are linearly interpolated in time while short-wave radiation is assumed to change with the solar
 223 zenith angle with maximum radiation occurring at solar noon. Following Arora (1997), the six-
 224 hourly precipitation amount (P , mm/6-hour) is used to estimate the number of wet half-hours
 225 (w_h) in a given six-hour period for $P > 0$ as

226
 227
$$w_h = \text{integer}(\max[1, \min(12, 2.6 \log(6.93 P))]). \quad (10)$$

Deleted:

229

230 The total precipitation amount is then distributed randomly but conservatively over these wet
231 half-hours. For instance, if seven out of 12 half hours intervals are calculated to be wet using
232 equation (10) then seven random numbers varying between 0 and 1 are generated and the six-
233 hourly precipitation amount is divided into seven parts in proportion to their respective random
234 numbers

235

236 Figure 1 shows the spatial distribution of mean annual precipitation and surface temperature over
237 the North American domain considered in this study. Mean annual precipitation values range
238 from less than 200 mm in the arid south-west United States and the high Arctic to more than
239 1500 mm on the Pacific coast. Mean annual temperature varies from around 24° C near the
240 southern limit of the domain in Mexico to less than -20° C in the Arctic tundra.

241

242 **2.3 Observation-based data**

243 **2.3.1 Fractional coverage of PFTs**

244

245 Observation-based estimates of fractional coverages of PFTs are based on a modified version of
246 the Wang et al. (2006) data set (hereafter WANG06) and the Moderate Resolution Imaging
247 Spectroradiometer land cover product (Friedl et al., 2013) (hereafter MODIS). These data are
248 used to evaluate the model results.

249

250 The WANG06 data set was developed for use by CTEM in simulations in which competition is
251 turned off and prescribed fractional coverage of PFTs is used. It combines observation- and
252 model-based data to estimate the annual change in fractional coverage of CTEM's nine PFTs
253 from 1850 to 2000. The Global Land Cover for the year 2000 (GLC2000), which is considered
254 as a base year for environmental assessment, divides the global land cover in 22 types is
255 available at 1 km resolution. WANG06 (their Table 2) mapped the GLC2000 data to CTEM's
256 nine PFTs aggregated to 0.5° resolution. The GLC2000 data were then extrapolated back to 1850
257 by adjusting the changes in crop area based on the then available Ramankutty and Foley (1999)
258 | [crop](#) data set. Here, we use a modified version of the WANG06 data set which is based on the

259 HYDE v.3.1 crop data set (Hurt et al., 2011) and generate an estimate of fractional coverage of
260 CTEM PFTs for the period 1850-2012.

261

262 The MODIS data set is based on the International Geosphere-Biosphere Programme (IGBP)
263 global vegetation data and University of Maryland's Science Data Set classification schemes at
264 0.25° spatial resolution. The data are derived from NASA HDF-EOS MODIS/Terra land cover
265 type. The data set is for the period 2001 to 2014 and contains 17 land cover types which we map
266 to CTEM's nine PFTs following the logic used in Wang et al. (2006) as shown in Table 2. The
267 fractional coverage of each of the nine CTEM PFT is first obtained at 0.25 degree resolution for
268 each year using the mapping scheme described in Table 2. These fractional coverages are then
269 re-gridded to the 1° spatial resolution for individual years. Finally, the data are averaged over the
270 period 2001-2014 to evaluate model results. MODIS data are known to exhibit substantial
271 interannual variability. Broxton et al. (2014), for instance, report that globally 40% of land pixels
272 show land cover change one or more times during 2001–2010 period. This does not necessarily
273 indicate changes in land cover but rather these differences are due to low accuracy in
274 categorizing the remotely sensed vegetation into one of the 17 MODIS land cover types, as
275 Broxton et al. (2014) note. This low accuracy is itself attributed to the fact that many landscapes
276 include mixtures of vegetation classes. Our re-gridding of fractional coverages to 1° spatial
277 resolution and averaging over the 2001-2014 time period to obtain climatology of land cover
278 alleviates some of the uncertainty since the effect of inaccurately classified land cover categories
279 is reduced due to both spatial and temporal averaging.

280

281 The separation of the broadleaf deciduous PFT into its drought and cold deciduous components
282 is performed via the approach used by WANG06. They assumed that below 24 °N deciduousness
283 is caused by soil moisture limitation and hence all broadleaf deciduous trees below this latitude
284 are drought deciduous, and above 34 °N deciduousness is caused by low temperatures and so all
285 broadleaf deciduous trees above this latitude are cold deciduous. Between 24 °N and 34 °N,
286 following WANG06 we assume a linear transition from drought deciduous to cold deciduous
287 trees. Finally, the separation of grasses into their C₃ and C₄ components is based on the
288 geographical distributions of the C₃ and C₄ fractions in the WANG06 data set.

289 **2.3.2 Gross primary productivity and LAI**

290

291 Observation-based estimates of gross primary productivity (GPP) are based on Beer et al. (2010).
292 These data are based on the ecosystem level GPP obtained using eddy covariance measurements
293 from more than 250 stations across the globe. Beer et al. (2010) extrapolated GPP values based
294 on these eddy covariance flux data ~~to the global scale using diagnostic models for the period~~
295 1982 – 2008, and the average over this time period is used to evaluate the model results. LAI
296 data used for validation are the same as those used by Anav et al. (2013) and are based on Zhu et
297 al. (2013) who use normalized difference vegetation index (NDVI) data from the Advanced Very
298 High Resolution Radiometer (AVHRR) satellite to calculate average LAI for the period 1981 –
299 2010.

Deleted: of GPP

300

301 **2.4 Experimental setup**

302

303 **2.4.1 Equilibrium pre-industrial simulation**

304

305 The equilibrium pre-industrial simulation was initialized from zero biomass and zero fractional
306 coverage for all non-crop PFTs. The fractions of C₃ and C₄ crop PFTs in each grid cell are
307 specified corresponding to year 1850 based on the HYDE 3.1 dataset. The model was then run
308 for 600 years driven by 1901-1925 CRU-NCEP climate data cycled repeatedly. These data do
309 not show any warming trend (Wen et al., 2011) as opposed to the later part of the 20th century.
310 Atmospheric CO₂ concentration was set to 285 ppm corresponding to the pre-industrial 1850
311 level. This pre-industrial equilibrium simulation yields initial conditions including fractional
312 coverages of PFTs and carbon in all the live and dead pools for the transient 1850-2010
313 simulation. The 600 years simulation is sufficient for fractional vegetation cover and carbon
314 pools to reach equilibrium.

315 **2.4.2 Transient historical simulation**

316

317 The transient historical simulation is performed for the period 1851-2010 and its carbon pools
318 and fractional coverage of non-crop PFTs are initialized from the equilibrium pre-industrial
319 simulation as mentioned above. The years 1851 to 1900 of this historical simulation are driven

321 with CRU-NCEP climate data corresponding to the period 1901-1925, cycled twice. For the
322 period 1901-2010 the climate data corresponding to each year are used. Time varying
323 concentrations of atmospheric CO₂ are supplied for the period 1851-2010 based on the values
324 used in the fifth Coupled Modelling Intercomparison Project (CMIP5,
325 <http://tntcat.iiasa.ac.at/RcpDb/>) which are extended past 2005 to 2010 based on data from the
326 National Oceanic and Atmospheric Administration
327 (ftp://aftp.cmdl.noaa.gov/products/trends/co2/co2_annmean_gl.txt). The annual time-varying
328 fractional coverages of C₃ and C₄ crop PFTs in each grid cell are based on the HYDE 3.1 dataset.
329 The crop fractions in a grid cell are not available for colonization and neither are they subject to
330 disturbance by fire. Competition between PFTs occurs over the remaining non-crop fraction of a
331 grid cell. As total crop fraction in a grid cell changes over time (based on the HYDE 3.1 dataset)
332 the fractional area available for competition also changes.

333

334 The simulated results are evaluated against their observation-based counterparts using averaged
335 values over the last 30 years of the simulation corresponding to the period 1981-2010. This is the
336 same and/or very close to the time period for modified WANG06 land cover data set (1981-
337 2010), Beer et al. (2010) GPP (1982-2008), and Zhu et al. (2013) LAI (1981-2010). The only
338 exception is the MODIS-based land cover data which are available for the 2001-2014 period.

339 **3 Results**

340

341 **3.1 Continental scale values of PFT coverage**

342

343 Figures 2a compares the simulated vegetation areas summed over our North American domain
344 with the WANG06 and MODIS observation-based estimates. In the absence of another measure
345 of uncertainty, we use the range between these two observation-based estimates and assess if
346 simulated areal coverage of a given land cover type lies within or outside this range. The
347 simulated total vegetated area over North America (14.8×10^6 km²) is very similar to the
348 modified WANG06 (14.4×10^6 km²) and MODIS derived (14.2×10^6 km²). At the most basic
349 tree-grass-bare ground level, the simulated areas are closer to the MODIS-based estimates, than
350 to the estimate based on the modified WANG06 data. The simulated area covered by tree PFTs

351 $(7.8 \times 10^6 \text{ km}^2)$ is 6% lower than the MODIS derived estimate $(8.2 \times 10^6 \text{ km}^2)$ and 21% lower
352 than WANG06 $(9.7 \times 10^6 \text{ km}^2)$. The simulated grass coverage $(4.7 \times 10^6 \text{ km}^2)$ is 35% higher
353 than the MODIS derived estimate $(3.5 \times 10^6 \text{ km}^2)$. Both simulated and MODIS-based estimates
354 of area covered by grass PFTs are, however, substantially higher than the WANG06 $(2.4 \times 10^6$
355 $\text{km}^2)$ estimate. Averaged over the North American region, the simulated partitioning of land area
356 (excluding cropland area) covered by trees, grasses and bare ground (45%, 27%, 28%) is much
357 closer to the MODIS based data (48%, 20% and 32%) than to the modified WANG06 based data
358 (56%, 14%, 30%).

359

360 Figure 2b shows a comparison of simulated areas of individual PFTs with observation-based
361 estimates. This is a more stringent test of the performance of the competition module of CTEM.
362 The observation-based estimates of areas of all individual PFTs are available for the modified
363 WANG06 dataset. The MODIS based estimates were derived based on the mapping of MODIS'
364 17 land cover types to CTEM PFTs as shown in Table 2, which itself is mostly based on
365 WANG06. In Figure 2b, the observation-based estimates show that needleleaf evergreen (NDL
366 EVG) and broadleaf cold deciduous (BDL DCD CLD) are the dominant tree PFTs across North
367 | America ~~and the model is able to reproduce this aspect~~. The simulated total area of the NDL
368 EVG tree PFT $(3.9 \times 10^6 \text{ km}^2)$ is 28% less than WANG06 $(5.3 \times 10^6 \text{ km}^2)$ and 15% less than the
369 MODIS based estimate $(4.7 \times 10^6 \text{ km}^2)$. The simulated total area of BDL DCD CLD tree PFT $(3$
370 $\times 10^6 \text{ km}^2)$ is 13% less than WANG06 $(3.4 \times 10^6 \text{ km}^2)$ and 3% greater than MODIS based $(2.9 \times$
371 $10^6 \text{ km}^2)$ estimate. Overall, the model is able to capture the areas covered by individual PFTs
372 reasonably well. However, differences remain between observations-based and simulated
373 estimates especially the larger simulated area for C_3 grasses than both observation-based
374 estimates. Reasons for these differences include limitations in the model but also the manner in
375 which remotely-sensed vegetation is categorized into broad-scale vegetation types and then
376 mapped onto CTEM's nine PFTs, as discussed later.

377

378 In both Figures 2a and 2b although simulated areal coverages at the basic tree-grass-bare ground
379 level and for individual PFTs (except for C_3 grasses) are comparable to observation-based

Deleted: which is also shown by the model

382 estimates they are outside the range defined by difference of the WANG06 and MODIS based
383 estimates.

384
385 Figure 2c shows the time series of simulated areas summed over the domain covered by tree and
386 grass PFTs, the total vegetated area and the remaining bare ground. The specified area covered
387 by crop PFTs, based on the HYDE 3.1 data set, is also shown and first increases over the
388 historical period and then stabilizes and in fact somewhat decreases in association with cropland
389 abandonment over the north-eastern United States. The increase in the crop area results in a
390 decrease in the area covered by tree and grass PFTs up until the time when the crop area
391 stabilizes around 1970. In the model, this causes land use change emissions associated with
392 deforestation. After this time, as vegetation productivity responds to increasing atmospheric CO₂
393 concentration, the area covered by tree PFTs increases somewhat and colonizes available bare
394 areas and those covered by grass PFTs. This leads to a small reduction in the area covered by
395 grass PFTs as well as bare ground and the associated increase in the total vegetated area.

396

397 **3.2 Geographical distribution of PFTs**

398

399 **3.2.1 Total vegetated and bare ground fractions**

400

401 Figures 3 and 4 compare the geographical distribution of simulated total vegetated and bare
402 fractions across North America with the two observation-based estimates derived from the
403 modified WANG06 and MODIS data sets. The two observation-based estimates are also
404 compared amongst themselves. The metrics used are averaged root mean square difference
405 (RMSD) and spatial correlations (R^2).

406

407 The observation-based geographical distribution of vegetated fraction in Figure 3 (middle
408 column) shows densely vegetated land over the eastern part of the continent and less vegetation
409 coverage over colder regions in the North and drier regions in the south-central and south-west
410 United States. These broad scale patterns are consistent with the precipitation and temperature
411 climatologies of the region (Figure 1). The model reasonably reproduces the observed vegetation
412 distribution (left panel) with some obvious limitations. Simulated vegetation cover is

413 underestimated across the arid south-west United States, Great Plains and part of the Canadian
414 Prairies (right panel) due to lower simulated fractional coverage of tree and grass PFTs over
415 these regions (shown in the next section). The model overestimates vegetation coverage in
416 Northern Canada because of higher simulated grass cover in the Arctic as discussed below in
417 more detail. The spatial correlation and RMSD when comparing simulated vegetated fraction to
418 both observation-based estimates are 0.79 and around 18%, respectively. The spatial correlation
419 and RMSD between the two observation-based estimates themselves are 0.86 and around 14%,
420 respectively.

Deleted: which are

421
422 The simulated and observation-based bare ground fractions across North America are compared
423 in Figure 4. The observation-based estimates show that bare ground fraction is higher in Arctic
424 Canada and Alaska where, of course, cold temperatures limit vegetation growth and in the south-
425 west United States, Great Plains and the Prairies where low rainfall limits vegetation growth
426 (Figure 1). The biases in simulated bare ground fraction mirror those in the simulated vegetated
427 fraction but in an opposite manner. The model underestimates bare ground fraction across Arctic
428 Canada due to higher simulated grass cover as discussed in the next section. The model
429 overestimates the bare ground fraction generally across the arid and semi-arid south-west United
430 States, Great Plains and the Prairies. The spatial correlations and RMSDs when comparing
431 simulated bare ground fraction to both observation-based estimates, and when comparing the two
432 observation-based data sets amongst themselves, are the same as those for the total vegetation
433 fraction in Figure 3.

Deleted:

Deleted: around 0.46 and around 18%, respectively. The spatial correlation and RMSD between the two observation-based estimates themselves are 0.68 and around 14%, respectively.

435 3.2.2 Tree and grass cover

436
437 Figure 5 compares the simulated tree cover with the two observation-based estimates. The model
438 reasonably reproduces the broad scale patterns including the Canadian boreal forest and the
439 temperate forests across the southeastern United States. However, the model simulates lower tree
440 cover across the western part of the continent compared to both observation-based estimates
441 particularly over the southwestern United States which is characterized by arid climate (Figure
442 1). The observation-based estimates do not particularly well agree over this region either. The
443 MODIS derived estimate suggests around 25% tree cover in the southwestern United States

451 while the WANG06 derived estimate suggests a tree cover of around 60% over a large area in
452 the region. The spatial correlation and RMSD when comparing simulated tree cover to both
453 observation-based estimates are around 0.68 and around 17%, respectively. The spatial
454 correlation and RMSD between the two observation-based estimates themselves are 0.75 and
455 around 15%, respectively. Possible reasons for differences between simulated and observation-
456 based estimates are discussed in detail in the discussion section and include the fact that the
457 CLASS-CTEM framework does not currently represent shrubs and there are limitations in the
458 observation-based data sets themselves. Shrubs are more prevalent in arid and semi-arid regions
459 where they are better suited to grow compared to both trees and grasses.

460
461 Figure 6 compares the geographical distribution of the simulated grass cover with the two
462 observation-based estimates. The broad geographical distribution of simulated grass cover
463 compares well with the two observation-based estimates with the notable exception of the Arctic
464 region including Alaska and northern Canada, where the model overestimates grass cover. This
465 overestimation of grass cover in the Arctic region is also the reason for the overestimation of
466 total vegetation fraction and the underestimation of bare fraction that was seen earlier in Figures
467 3 and 4 respectively.

468
469 As shown in Figure 6, the spatial correlation and RMSD when comparing simulated grass cover
470 to both observation-based estimates lie between 0.33 and 0.38 and between around 15-17%,
471 respectively. The spatial correlation and RMSD between the two observation-based estimates
472 themselves are 0.54 and around 9%, respectively. The two observation-based estimates disagree
473 most markedly over the western half of the United States where the MODIS derived estimates of
474 grass cover are higher.

475
476 **3.2.3 Needleleaf evergreen and broadleaf cold deciduous trees**

477
478 Figures 7a and 7b compare the geographical distribution of NDL EVG and BDL DCD CLD
479 trees, respectively, with their observation-based estimates. These two are the primary tree PFTs
480 which exist in the North American domain considered here.

481

482 In Figure 7a, the overall simulated coverage of NDL EVG trees is lower than both observation-
483 based estimates as was also seen in Figure 2b. The simulated values are primarily lower in
484 western Canada and over a large area in the western United States according to estimates based
485 on the modified WANG06 data set. This is also the case along the wide swath of the Canadian
486 boreal forest. The model overestimates the coverage of NDL EVG trees in the eastern United
487 States. The spatial correlation and RMSD when comparing simulated coverage of NDL EVG
488 trees to both observation-based estimates lie between 0.36 and 0.40 and between around 16-17%,
489 respectively. The spatial correlation and RMSD between the two observation-based estimates
490 themselves are 0.52 and around 16%, respectively.

491
492 The geographical distribution of BDL DCD CLD trees is compared with its observation-based
493 estimates in Figure 7b. Although the simulated domain summed area of BDL DCD CLD trees (3
494 $\times 10^6$ km²) is comparable to estimates based on the modified WANG06 (3.4×10^6 km²) and
495 MODIS (2.9×10^6 km²) data sets, there are two primary limitations in its simulated geographical
496 distribution. First, the simulated values are generally overestimated in Canadian boreal forests
497 and underestimated in the eastern United States. Second, the model simulates near zero coverage
498 in the arid south-western United States. The spatial correlation and RMSD when comparing
499 simulated coverage of BDL DCD CLD trees to both observation-based estimates are around 0.3
500 and around 12%, respectively. The spatial correlation and RMSD between the two observation-
501 based estimates themselves are 0.60 and around 8%, respectively.

502

503 3.2.4 C₃ and C₄ grasses

504

505 Figures 8a and 8b compare the simulated geographical distribution of C₃ and C₄ grasses with
506 observation-based estimates.

507

508 In Figure 8a, the most obvious limitation of the model is its excessive simulated grass coverage
509 in Alaska and in Arctic Canada. Other than this, the model reproduces the broad geographical
510 distribution of C₃ grasses including the Great Plains of United States and the Canadian Prairies,
511 where a large extent of grasslands is observed. The overestimated grass coverage at high
512 latitudes leads to a total simulated C₃ grass area (4.4×10^6 km²) that is higher than estimates

513 based on the modified WANG06 ($1.9 \times 10^6 \text{ km}^2$) and MODIS ($2.8 \times 10^6 \text{ km}^2$) data sets. The
514 spatial correlation and RMSD when comparing simulated coverage of C₃ grasses to both
515 observation-based estimates lie between 0.34-0.38 and between around 15-17%, respectively.
516 The spatial correlation and RMSD between the two observation-based estimates themselves are
517 0.54 and around 12%, respectively.

518
519 Figure 8b shows the distribution of C₄ grasses which mostly occur in the tropics and do not
520 occupy large areas in North America (as was also seen in Figure 2b). The modelled geographical
521 distribution of C₄ grasses is larger than observation-based estimates but the absolute fractions
522 remain small so that the simulated area covered over the whole domain ($0.35 \times 10^6 \text{ km}^2$) is
523 actually smaller than estimates based on the modified WANG06 ($0.45 \times 10^6 \text{ km}^2$) and MODIS
524 ($0.7 \times 10^6 \text{ km}^2$) data sets. The spatial correlation and RMSD when comparing simulated
525 coverage of C₄ grasses to both observation-based estimates lie between 0.12-0.16 and between
526 around 3-5%, respectively. The spatial correlation and RMSD between the two observation-
527 based estimates themselves are 0.62 and around 5%, respectively.

528
529 We do not compare the spatial distribution of broadleaf evergreen (BDL EVG) and broadleaf
530 drought deciduous (BDL DCD DRY) trees with the two observation-based estimates for three
531 reasons: 1) the geographical distribution of these PFTs is limited to a small total area in our
532 domain, 2) the geographical distribution of the BDL EVG tree PFT based on observations cannot
533 be directly compared to simulated values because, when mapping land cover types to CTEM
534 PFTs in WANG06, evergreen shrubs (which exist much farther north than 30 °N) are assigned to
535 the BDL EVG tree PFT, and 3) the geographical distribution of the BDL DCD DRY tree PFT in
536 the observation-based data sets is based on the arbitrary latitudinal thresholds of 24 °N and 34 °N
537 as mentioned earlier.

538 539 3.3 LAI and GPP

540
541 Figure 9 compares the geographical distribution of simulated LAI and GPP with observation-
542 based estimates for the present day. In Figure 9a, the simulated geographical distribution of LAI
543 compares well with the observation-based estimates. The spatial correlation and RMSD between

Deleted: ¶
Broadleaf evergreen and drought deciduous trees¶

¶
The least prevalent PFTs in the North American domain considered here are broadleaf evergreen (BDL EVG) and broadleaf drought deciduous (BDL DCD DRY) trees. As they are represented in the model these are primarily tropical PFTs and hence generally do not exist above around 30 °N (see Figure 9), according to the bioclimatic limits used in the model for tree PFTs (Melton and Arora, 2016). In our simulations, these PFTs therefore exist near the southern edge of the United States. We do not evaluate spatial correlation and RMSD for these PFTs compared to the

Deleted: the

Deleted: 10

Deleted: 10a

565 simulated and observation-based estimates are 0.74 and 0.81 m^2/m^2 , respectively. The domain
566 averaged simulated LAI of 2.5 m^2/m^2 is higher than the observation-based estimate of 2.1 m^2/m^2 .
567 The model captures the broad geographical patterns with higher LAI over the boreal forest
568 region in Canada and also in the eastern United States similar to observations. However, some
569 differences remain particularly over the drier southwest United States where the model simulates
570 bare ground with negligible LAI but observations suggest a small LAI of around 1 m^2/m^2 . In
571 contrast, the model slightly overestimates LAI over northern and Arctic Canada where it
572 simulates a higher fractional coverage of C_3 grasses, as seen earlier.

573

574 Consistent with the geographical distribution of LAI, the simulated GPP is overestimated in the
575 eastern United States and the Canadian boreal forest (Figure 9b). The broad geographical
576 distribution of GPP, similar to LAI, is consistent with the observation-based estimates. The
577 spatial correlation and RMSD between simulated and observation-based estimates are 0.78 and
578 225 $\text{gC}/\text{m}^2\cdot\text{year}$, respectively. The domain averaged simulated GPP of 737 $\text{gC}/\text{m}^2\cdot\text{year}$ is higher
579 than the observation-based estimate of 628 $\text{gC}/\text{m}^2\cdot\text{year}$. As with LAI, the simulated GPP is lower
580 than observations over the drier southwest region of the United States where the model simulates
581 more bare ground than observation-based estimates, and the model overestimates GPP over the
582 northern and Arctic Canada.

Deleted: 10b

583

584 Figure 10 shows the time series of annual domain averaged GPP, LAI, net primary productivity
585 (NPP) and domain summed net biome productivity (NBP). The NBP term is essentially the net
586 atmosphere-land CO_2 flux which is the result of all terrestrial ecosystem processes including
587 photosynthesis, autotrophic and heterotrophic respiration, fire and land use change. NBP values
588 of zero indicate that the system is in equilibrium such that carbon gained by photosynthesis is
589 equal to carbon lost by respiration and other processes. Simulated GPP, LAI and NPP all show
590 an increase over the 20th century due to the increase in atmospheric CO_2 concentration and the
591 associated change in climate. The increase in CO_2 drives the increase in GPP and subsequently in
592 NPP and LAI through the CO_2 fertilization effect. The net result of this gradually increasing NPP
593 is that the terrestrial ecosystems become a sink of carbon and this is seen in the resulting positive
594 values of NBP. The simulated sink over the North American domain for the periods 1990-2000
595 and 2000-2010 is around 0.4 and 0.5 $\text{Pg C}/\text{year}$, respectively. Crevoisier et al. (2010) compare

Deleted: 1

598 the carbon sink over the North American region from five studies (their Table 1) for time periods
599 in the 1990s and 2000s. These reported sinks vary from 0.81 ± 0.72 to 1.26 ± 0.23 Pg C/year for the
600 period 1992-1996, 0.58 Pg C/yr for the period 2001-2006 and Crevoisier et al. (2010) themselves
601 estimate a value of 0.51 ± 0.41 Pg C/yr for the period 2004-2006. The sinks simulated by
602 CLASS-CTEM over the 1990s and 2000s are broadly consistent with these estimates.

603

604 **3.4 Added value of finer spatial resolution**

605

606 Figure 11 assesses the added value of running the model and performing competition between
607 PFTs at the 1° spatial resolution used in this study compared to the 3.75° resolution used in
608 Melton and Arora (2016) study which evaluated the performance of CLASS-CTEM's
609 competition module at the global scale. For Figure 11, the Melton and Arora (2016) results were
610 extracted for the North American domain used in this study and observation-based estimates of
611 fractional coverage of tree, grass and total vegetation from the modified WANG06 land cover
612 product were re-gridded to the 3.75° resolution. The resulting spatial correlations and RMSDs
613 between the simulated and the WANG06 estimates for fractional coverage of tree, grass and total
614 vegetation, at the two spatial resolutions, are summarized in Figure 11. When compared to the
615 modified WANG06 data the RMSDs are somewhat lower (Figure 11a), and spatial correlations
616 (Figure 11b) are slightly higher for model's implementation at 3.75° resolution, compared to
617 model's implementation at 1° resolution. This indicates that the model's performance is slightly
618 better at the coarser 3.75° resolution. Recall that competition between PFTs occurs over the non-
619 crop fraction of each grid cell. For this reason, we do not perform this analysis for MODIS based
620 land cover product because the crop areas that are specified in the model are exactly same as
621 those in the modified WANG06 land cover product making comparison of simulated and
622 observation-based fractional coverages of PFTs more consistent for the modified WANG06 land
623 cover product.

624

625 **4 Discussion**

626

627 Competition between PFTs, that determines their fractional coverage, is one of the several
628 processes that the CLASS-CTEM modelling framework simulates. Other than competition

Deleted: ¶

630 between PFTs, terrestrial ecosystem processes of photosynthesis, autotrophic and heterotrophic
631 respiration, allocation of carbon from leaves to stem and root components, dynamic leaf
632 phenology, fire, and land use change are also modelled. These aspects of the model have been
633 evaluated at point (Arora, 2003; Arora and Boer, 2005; Melton et al., 2015), regional (Garnaud et
634 al., 2015; Peng et al., 2014; Arora et al., 2016) and global (Arora and Boer, 2010; Melton and
635 Arora, 2014; Melton and Arora, 2016) scales. A typical model evaluation exercise at the global
636 scale compares model simulated geographical and latitudinal distribution of GPP, vegetation
637 biomass, and soil carbon with their respective observation-based estimates such as those from
638 Beer et al. (2010), Ruesch and Holly (2008) and Harmonized World Soil Database
639 (FAO/IIASA/ISRIC/ISS-CAS/JRC, 2012). Model evaluation exercises help in identifying model
640 limitations but also yield opportunities to improve model performance by tuning model
641 parameters. CLASS-CTEM model also participated in the 2016 TRENDY intercomparison of
642 terrestrial ecosystem models whose results contributed to the global carbon project (Le Quéré et
643 al., 2016). The competition module of the CLASS-CTEM modelling framework has been
644 previously evaluated at point scales (Arora and Boer, 2006; Shrestha et al., 2016). In addition to
645 assessing fractional coverage at which PFTs equilibrate, these point scale evaluations also assess
646 the time the PFTs take to reach their equilibrium fractional coverages against empirical data and
647 if the succession patterns are realistically simulated (e.g. grasses should colonize a given area
648 before trees invade the area covered by grasses). This manuscript focusses on evaluation of the
649 competition module of the CLASS-CTEM modelling framework at a regional scale.

Deleted: ¶

651 Dynamically simulated fractional coverages of PFTs adds another degree of freedom to a model
652 compared to the case where the fractional coverages of its PFTs are specified. This is a more
653 stringent test of a model's performance. Errors in the simulated geographical distribution of
654 PFTs will, of course, lead to corresponding errors in the geographical distribution of primary
655 terrestrial ecosystem carbon pools and fluxes. Yet, the CLASS-CTEM model is broadly able to
656 reproduce the geographical distributions of GPP and LAI. Limitations, of course, remain. In
657 particular, the simulated LAI and GPP are high in Alaska and in northern and Arctic Canada, and
658 these variables are lower than their observation-based estimates in arid regions of the western
659 United States. The simulated fractional vegetation coverage reflects these patterns.

Deleted: Allowing a terrestrial ecosystem model to

Deleted: its

Deleted: the

666 It is difficult to conclusively determine whether these model limitations are due to the limitations
667 in the biogeochemistry parameterizations of the model for its existing PFTs or the simple
668 structural limitation that the model does not represent shrub, moss and lichen PFTs. Shrubs are
669 adapted to grow in arid and semi-arid regions, whether in cold or hot climates (where neither
670 grasses nor trees are able to grow) and their representation in the model would likely help to
671 increase the fractional vegetation cover in arid regions including those in the western United
672 States. At high latitudes grass growth is inhibited by mosses and lichens which flourish in cold
673 and damp conditions. A representation of moss and lichen PFTs and improved representation of
674 permafrost in the model would likely help to decrease simulated grass coverage in Arctic
675 regions. In the current version of the CLASS-CTEM model bioclimatic limits are used only for
676 tree PFTs to ensure that these PFTs do not venture outside their pre-determined bioclimatic
677 zones. In the model, bioclimatic limits are not used for grasses and their geographical
678 distribution is entirely the result of plant physiological processes and their competitive
679 interactions with the tree PFTs and amongst themselves. Since, in the Arctic region, grasses do
680 not face competition from tree PFTs, and moss and lichen PFTs are not represented in the model,
681 they are free to increase their expanse – climate permitting, of course. Another possible reason
682 for higher than observed grass coverage in the Arctic region is that in the current implementation
683 of CLASS only three permeable soil layers with maximum thicknesses of 0.1, 0.25 and 3.75 m
684 are represented and a boundary condition of zero heat flux is assumed across the bottommost
685 layer. This simple representation does not allow to model permafrost realistically. Permafrost is
686 more realistically modelled with multiple permeable and impermeable (extending into the bed
687 rock) layers that go sufficiently deep (> 30 m at least) to capture the slow evolution of soil
688 temperatures in response to climate warming (Teufel et al., 2017). The current set up of three
689 layers that go only 4.1 m deep produces soil temperatures that are warmer than in the set up
690 when permeable and impermeable layers are sufficiently deep and produces permafrost extent
691 that is lower than observation-based estimates (Koven et al., 2013). It is likely that warmly
692 biased soil temperatures in the current set up contribute to promote grass growth and allow it to
693 cover a larger area in the Arctic region than would be the case when permafrost is more
694 realistically modelled.

695

696 The lower than observed fractional vegetation cover in the arid and semi-arid regions of the
697 western United States, however, may not solely be due to model limitations alone. Here, we
698 argue that the manner in which remotely sensed land cover types are mapped to CTEM PFTs,
699 and the errors in calculating bare ground fraction in remotely sensed products also contribute to
700 mismatch between modelled and observation-based values of fractional vegetation cover. We
701 illustrate this by comparing the functional relationship between LAI and total vegetation cover.
702 Figure 12a shows this relationship for model simulated values. As expected, as LAI increases so
703 does the total vegetation cover. The relationship between these two variables is fairly tight in the
704 model and the green line is an exponential fit. The red dots in the figure correspond to grid cells
705 that lie in the region identified in the inset in Figure 12d and broadly correspond to the western
706 half of the United States. Figures 12b and 12c show the same relationship but between the
707 observation-based estimate of LAI from Zhu et al. (2013) (as mentioned in Section 2.3.2) and the
708 total vegetation cover based on the WANG06 and MODIS derived land cover data sets,
709 respectively. The blue and magenta lines in Figures 12b and 12c are the corresponding
710 exponential fits. When compared with Figure 12a, Figures 12b and 12c show much more scatter
711 around the fitted curves, and the overall relationship appears to break down for the red dots
712 corresponding to the grid cells in the western United States. A careful look at the red dots in
713 Figures 12b and 12c shows that the observation-based vegetation cover in the Western United
714 States for a large fraction of grid cells is around 60% regardless of the observation-based LAI
715 which ranges between 0.1 and 1.5 m^2/m^2 . Clearly, it is physically unrealistic to achieve fractional
716 vegetation coverage of 60% below LAI values of 0.6 m^2/m^2 (the m^2/m^2 unit implies m^2 of leaf
717 area per m^2 of ground area) and this indicates that the fractional vegetation cover in this region is
718 likely overestimated in both observation-based data sets.

719
720 There are at least two ways in which errors in total vegetation cover can occur. The first relates
721 to the method by which the fractional vegetation cover is calculated for the land cover types in
722 the original remotely sensed land cover products: that is, for the 22 land cover types in the
723 GLC2000 data set upon which the WANG06 data are based and the 17 land cover types in the
724 MODIS data set. An example of such an error for arid regions is illustrated by Lawley et al.
725 (2014) who suggest that the MODIS soil fractional cover product, at least in its present form, is
726 unsuited to monitoring sparsely vegetated arid landscapes and generally unable to separate soil

727 from vegetation in situations where normalized difference vegetation index (NDVI) is low. The
728 second way in which errors are introduced is through the mapping of the remotely sensed land
729 cover types to the CTEM PFTs following Table 2 of WANG06 for the GLC2000 land cover
730 types, and following Table 2 in this manuscript for the MODIS land cover types. This mapping
731 is based on available information in the literature but is also based on expert judgement which
732 introduces subjectiveness. For instance, it is debatable what fraction of the “open shrublands”
733 MODIS land cover type, which exists over much of the arid southwestern United States, is in
734 fact bare ground. In Table 2, we have allocated a fraction of 0.4 of “open shrublands” to bare
735 ground following WANG06. Had WANG06 allocated a higher value than this to bare ground,
736 our simulated values would have compared better with the observation-based values of bare
737 ground fraction over arid regions. Nevertheless this would not have changed the relationship, or
738 rather the lack thereof, between the observation-based estimates of LAI and the total vegetation
739 cover in the western half of the United States seen in Figures 12b and 12c.

Deleted: value

Deleted: to this fraction

740
741 Both model and observation-based results are also affected by a common limitation associated
742 with peatlands which exists in the Hudson Bay lowlands region. Both the GLC2000 data set,
743 upon which the modified WANG06 land cover product is based, and the MODIS land cover data
744 do not represent peatland vegetation. In these data sets the peatland vegetation is classified either
745 as grasses, shrubs or trees. The model also does not represent peatlands and as a result the model
746 grows trees and grasses in regions where peatlands exists. Work is under way to incorporate a
747 peatland model developed for CLASS-CTEM (Wu et al., 2016) into our modelling framework.

748
749 The simulated areas covered by the primary two tree PFTs (NDL EVG and BDL DCD COLD)
750 have their weaknesses but large differences also exist between the two observation-based
751 estimates especially for the NDL EVG PFT. Modelling competition between two tree PFTs is
752 much more difficult than between trees and grasses. In the latter case trees are always considered
753 superior to grasses, but in the case of competition between two tree PFTs the superiority is based
754 on parameterized colonization rates which depend on simulated NPP. Based on comparisons
755 with observation-based estimates, the main limitation in model results here is that the model
756 overestimates the coverage of NDL EVG trees, and underestimates the coverage of BDL DCD
757 COLD trees in the eastern United States, while the opposite is true in western Canada. The

Deleted: ¶

761 model, of course, does not represent individual species, while in the real world competition
762 occurs at the species level that is modulated by soils and nutrient availability. An example that
763 illustrates this limitation of the model is the Jack pine tree species which occupies ecological
764 niche of nutrient poor soils in Boreal Canada (e.g. see Ste-Marie et al., 2007). The coupling of
765 carbon and nutrient cycles is currently not represented in CLASS-CTEM and optimizing model
766 parameters for hundreds of species is currently extremely difficult given limited available data at
767 the species level. Most likely before the model is applied at the species level, as a first step, the
768 number of PFTs represented in the model should be increased. An example of how additional
769 PFTs in the CLASS-CTEM framework can lead to improved model performance is illustrated by
770 Peng et al. (2014). This application of the model shows how sub-dividing the NDL EVG PFT
771 into coastal and interior types for the province of British Columbia in Canada leads to
772 improvement in simulated LAI and GPP. A recent attempt to explicitly represent physiological
773 process in a model to simulate competition between needleleaf and broadleaf cold deciduous
774 trees at a regional scale is illustrated in (Fisher et al., 2015) who incorporated the concepts from
775 the Ecosystem Demographics (ED) model into the community land model – dynamic vegetation
776 model (CLM-DGVM). Their results provide some interesting insights; however, validation of
777 this approach at the global scale over a wide range of PFTs remains challenging.

778
779 Finally, one of the objectives of this study was to evaluate if resolving climate niches by
780 performing CLASS-CTEM simulation at a finer resolution of 1° in this study allowed improved
781 simulation of geographical distribution of PFTs than in the Melton and Arora (2016) study that
782 evaluated the competition module of the CLASS-CTEM model at 3.75° spatial resolution at the
783 global scale. Figure 11 addresses this objective and shows that while the spatial correlations and
784 RMSDs between the simulated and the modified WANG06 land cover product for fractional
785 coverage of tree, grass and total vegetation are fairly similar for the model outputs at 1° and
786 3.75° resolutions, these metrics are somewhat better for model's application at the coarser 3.75°
787 resolution. One possible reason for the slightly worse model performance at the finer resolution
788 is that while climate niches are resolved better at the finer resolution the model does not have the
789 additional differentiation in PFTs (the number of model PFTs is still nine) that is required to gain
790 benefit from the resolved climate niches. In addition, comparing Melton and Arora (2016) results
791 over North America with ones obtained here we note that the primary model limitations remain

Deleted: .

Deleted: One

Deleted: ,

Deleted: s

Deleted: 2

Deleted: through 4 of Melton and Arora (2016) compare simulated geographical distributions of PFTs with WANG06 data

Deleted: . C

Deleted: their

802 unchanged in the application of the model at both spatial resolutions. These include lower
803 simulated fractional vegetation coverage in the arid south-west North American region and
804 higher in the Arctic region (due to higher grass coverage). In addition, in both applications of the
805 model the differences in simulated geographical distribution of NDL EVG and BDL DCD CLD
806 PFTs, compared to the WANG06 land cover data, are also similar. Model differences, compared
807 to the WANG06 data, therefore remain more or less similar in the application of the model at
808 both spatial resolutions. These results are, however, based on offline applications of the CLASS-
809 CTEM model where it is driven by reanalysis data. In a fully-coupled simulation where CLASS-
810 CTEM is coupled to an atmospheric model it is possible that model performance at low spatial
811 resolution is different from its performance at high spatial resolution.
812

813 The comparison between observation-based and simulated fractional coverages is the most
814 robust at the basic tree-grass-bare ground level. The subjectiveness introduced in the process of
815 mapping remotely sensed land cover types to the PFTs represented in a model, as mentioned
816 above, makes the comparison of simulated and observation-based fractional coverages for
817 individual PFTs less robust. Nevertheless, comparisons with observations allow useful insights
818 into model limitations as we have seen here.

819

820

821 **5 Summary and conclusions**

822

823 This study evaluates the CLASS-CTEM simulated fractional coverages of PFTs, when driven
824 with observed meteorological forcing, against the observation-based estimates from MODIS and
825 the modified WANG06 data sets over the North American region. In the past, performance of the
826 competition module of the CLASS-CTEM modelling framework has been assessed at global
827 scale, at a coarse spatial resolution of 3.75° (Melton and Arora, 2016), as well as at point scale,
828 for a range of locations across the globe (Shrestha et al., 2016). Our objective here was to assess
829 the performance of the CLASS-CTEM competition module at a higher spatial resolution of 1°
830 over North America. To achieve this objective we compared simulated present day geographical
831 distributions of fractional coverages of PFTs, but also LAI and GPP with their observation-based
832 estimates.

Deleted: climate

834

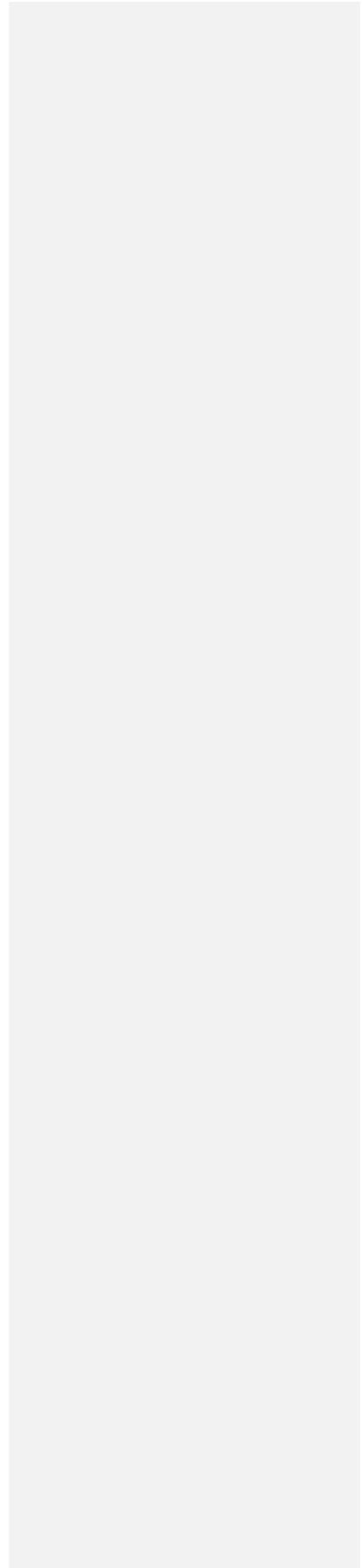
835 The CLASS-CTEM modelling framework is generally able to reproduce the dominant features
836 of the geographic distribution of PFT coverage, and LAI and GPP over the North American
837 region. After 1960, the model simulates increasing GPP and LAI in response to changing climate
838 as well as increased atmospheric CO₂ concentrations and the resulting sink for the 1990s and
839 2000s is broadly consistent with other estimates.

840

841 The simulated geographical distribution of PFTs, when compared to observation-based
842 estimates, show two primary limitations which are excessive grass cover in the Arctic region and
843 low vegetation cover in the arid western United States, although for the latter the observation-
844 based estimates themselves may have their own weaknesses. There are three main factors in the
845 CLASS-CTEM modelling framework that may have contributed to these differences: 1) the
846 absence of a shrub PFT, which we believe is the reason for low simulated vegetation coverage in
847 the arid to semi-arid western United States, 2) the absence of moss and lichen PFTs that may
848 inhibit the establishment of grasses, and 3) probably a lack of sensitivity of C₃ grasses to high
849 latitude climate and an inadequate representation of permafrost. Future model developments will
850 focus on these aspects with a view to improving model performance.

851

852



854 **References:**

855 Anav, A., Friedlingstein, P., Kidston, M., Bopp, L., Ciais, P., Cox, P., Jones, C., Jung, M.,
856 Myneni, R., and Zhu, Z.: Evaluating the land and ocean components of the global carbon
857 cycle in the CMIP5 earth system models, *J. Climate*, 26, 6801-6843, doi:10.1175/JCLI-
858 D-12-00417.1, 2013.

859
860 Arora, V. K.: Land surface modelling in general circulation models: a hydrological perspective,
861 PhD Thesis, University of Melbourne, Australia, 1997.

862
863 [Arora, V.K.: Simulating energy and carbon fluxes using coupled land surface and terrestrial](#)
864 [ecosystem models, *Agricultural and Forest Meteorology*, 118\(1-2\), 21-47, 2003.](#)

865
866 Arora, V. K. and Boer, G. J.: A representation of variable root distribution in dynamic vegetation
867 models, *Earth Interactions*, 7, 1-19, 2003.

868
869 Arora, V. K. and Boer, G. J.: A parameterization of leaf phenology for the terrestrial ecosystem
870 component of climate models, *Glob. Change Biol.*, 11, 39-59, 2005.

871
872 Arora, V. K. and Boer, G. J.: Simulating Competition and Coexistence between Plant Functional
873 Types in a Dynamic Vegetation Model, *Earth Interactions*, 10, 1-29, 2006.

874
875 [Arora, V.K. and G.J. Boer: Uncertainties in the 20th century carbon budget associated with land](#)
876 [use change, *Global Change Biology*, 16\(12\), 3327-3348, 2010.](#)

877
878 Arora, V. K., Boer, G. J., and Friedlingstein, P. E. A.: Carbon-concentration and carbon-climate
879 feedbacks in CMIP5 earth system models, *J. Climate*, 26, 5289-5314, 2013.

880
881 [Arora, V. K., Y. Peng, W. A. Kurz, J. C. Fyfe, B. Hawkins, and A. T. Werner: Potential near-](#)
882 [future carbon uptake overcomes losses from a large insect outbreak in British Columbia,](#)
883 [Canada, *Geophys. Res. Lett.*, 43, doi:10.1002/2015GL067532, 2016.](#)

884
885 Beer, C., Reichstein, M., Tomelleri, E., Ciais, P., Jung, M., Carvalhais, N., Rodenbeck, C.,
886 Arain, M. A., Baldocchi, D., Bonan, G. B., Bondeau, A., Cescatti, A., Lasslop, G.,
887 Lindroth, A., Lomas, M., Luysaert, S., Margolis, H., Oleson, K. W., Rouspard, O.,
888 Veenendaal, E., Vivoy, N., Williams, C., Woodward, F. I., and Papale, D.: Terrestrial
889 gross carbon dioxide uptake: global distribution and covariation with climate, *Science*,
890 329, 834-838, doi:10.1126/science.1184984, 2010.

891
892 Bonan, G. B.: Forests and climate change: Forcings, feedbacks, and the climate benefits of
893 forests, *Science*, 320, 1444-1449, doi:10.1126/science.1155121, 2008.

894
895 Box, E. O.: Plant functional types and climate at the global scale, *J. Veg. Sci.*, 7, 309-320,
896 doi:10.2307/3236274, 1996.

897

898 Brentnall, S. J., Beerling, D. J., Osborne, C. P., Harland, M., Francis, J. E., Valdes, P. J., and
899 Wittig, V. E.: Climatic and ecological determinants of leaf lifespan in polar forests of the
900 high CO₂ Cretaceous 'greenhouse' world, *Glob. Change Biol.*, 11, 2177-2195, 2005.
901

902 Broxton, P., X. Zeng, D. Sulla-Menashe, and P. Troch, 2014: A Global Land Cover Climatology
903 Using MODIS Data. *J. Appl. Meteor. Climatol.*, 53, 1593–1605, doi: 10.1175/JAMC-D-
904 13-0270.1.
905

906 Cox, P. 2001: Description of the "TRIFFID" Dynamic Global Vegetation Model. Tech. Note 24.
907

908 Cramer, W., Bondeau, A., Woodward, F. I., Prentice, I. C., Betts, R. A., Brovkin, V., Cox, P. M.,
909 Fisher, V., Falloon, P. D., Foley, J., Friend, A. D., Kucharik, C., Lomas, M. R.,
910 Ramankutty, N., Sitch, S., Smith, B., White, A., and Molling-Young, C.: Global response
911 of terrestrial ecosystem structure and function to CO₂ and climate change: results from
912 six dynamic global vegetation models, *Global Change Biology*, 7, 357-373, 2001.
913

914 Crevoisier, C., Sweeney, C., Gloor, M., Sarmiento, J. L., and Tans, P. P.: Regional US carbon
915 sinks from the three-dimensional atmospheric CO₂ sampling, *PANAS*, 107, 18348-
916 18353, DOI: 10.1073/pnas.0900062107, 2010.
917

918 Dai, Y., Zeng, X., Dickinson, R. E., and Coauthors: Common Land Model (CLM), Technical
919 documentation and user's guide. [Available online at
920 <http://climate.eas.gatech.edu/dai/clmdoc.pdf>.], 2001.
921

922 [FAO/IIASA/ISRIC/ISS-CAS/JRC: Harmonized World Soil Database \(version 1.2\), available at:
923 \[http://www.fao.org/soils-portal/soil-survey/soil-maps-and-databases/harmonized-world-
924 soil-database-v12/en/\]\(http://www.fao.org/soils-portal/soil-survey/soil-maps-and-databases/harmonized-world-soil-database-v12/en/\) \(last access: 20 January 2016\), 2012.](http://www.fao.org/soils-portal/soil-survey/soil-maps-and-databases/harmonized-world-soil-database-v12/en/)
925

926 Fisher, R. A., Muszala, S., Versteinstein, M., Lawrence, P., Xu, C., McDowell, N. G., Knox, R.
927 G., Koven, C., Holm, J., Rogers, B. M., Spessa, A., Lawrence, D., and Bonan, G.: Taking
928 off the training wheels: the properties of a dynamic vegetation model without climate
929 envelopes, *CLM4.5(ED)*, *Geosci. Model Dev.*, 8, 3593-3619, doi:10.5194/gmd-8-3593-
930 2015, 2015.
931

932 Friedl, M., Strahler, A., Schaaf, C., Hodges, J. C. F., and Salomon, J., 2013.: Binary MODIS
933 MOD12C1 0.25 Degree Land Cover Climate Modeler Grid. Available at
934 [\[http://duckwater.bu.edu/lc/\]](http://duckwater.bu.edu/lc/) from the Department of Geography, Boston University,
935 Boston, Massachusetts, USA., 2013.
936

937 Friedlingstein, P., Cox, P., Betts, R., Bopp, L., Von Bloh, W., Brovkin, V., Cadule, P., Doney,
938 S., Eby, M., Fung, I., Bala, G., John, J., Jones, C., Joos, F., Kato, T., Kawamiya, M.,
939 Knorr, W., Lindsay, K., Matthews, H. D., Raddatz, T., Rayner, P., Reick, C., Roeckner,
940 E., Schnitzler, K.-G., Schnur, R., Strassmann, K., Weaver, A. J., Yoshikawa, C., and
941 Zeng, N.: Climate–carbon cycle feedback analysis: Results from the C4MIP model
942 intercomparison, *J. Climate*, 19, 3337-3353, 2006.
943

- 944 Friend, A. D., Chard, Lucht, W., Rademacher, T., Keribin, R., Betts, R., Cadule, P., Ciais, P.,
945 Clark, D. B., Dankers, R., Falloon, P. D., Ito, A., Kahana, R., Kleidon, A., Lomas, M. R.,
946 Nishina, K., Ostberg, S., Pavlick, R., Peylin, P., Schaphoff, S., Vuichard, N.,
947 Warszawski, L., Wiltshire, A., and Woodward, F. I.: Carbon residence time dominates
948 uncertainty in terrestrial vegetation response to future climate and atmospheric CO₂,
949 Proc. Natl. Acad. Sci. USA, 111, 3280-3285, 2013.
- 950
- 951 Garnaud, C., Sushama, L., and Verseghy, D.: Impact of interactive vegetation phenology on the
952 Canadian RCM simulated climate over North America, Climate Dynamics, 45, 1471-
953 1492, doi:10.1007/s00382-014-2397-9, 2015.
- 954
- 955 Gobron, N., Belward, A., and Knorr, W.: Monitoring biosphere vegetation 1998-2009, Geophys.
956 Res. Lett., 37, L15402, 2010.
- 957
- 958 Hurtt, G. C., Chini, L. P., Frolking, S., Betts, R. A., Feddema, J., Fischer, G., Fisk, J. P.,
959 Hibbard, K., Houghton, R. A., Janetos, A., Jones, C. D., Kindermann, G., Kinoshita, T.,
960 Klein Goldewijk, K., Riahi, K., Shevliakova, E., Smith, S., Stehfest, E., Thomson, A.,
961 Thornton, P., Van Vuuren, D. P., and Wang, Y. P.: Harmonization of land-use scenarios
962 for the period 1500-2100: 600 years of global gridded annual land-use transitions, wood
963 harvest, and resulting secondary lands, Climate Change, 109, 117-161, 2011.
- 964
- 965 Kramer, P. J. and Kozlowski, T. T., 1979: Physiology of woody plants. Academic press, 1979.
- 966
- 967 Koven, C. D., Riley, W. J. and Stern, A.: Analysis of Permafrost Thermal Dynamics and
968 Response to Climate Change in the CMIP5 Earth System Models, J. Clim., 26(6), 1877-
969 1900, 2013.
- 970
- 971 Lawley, E. F., Lewis, M. M., and Ostendorf, B.: Evaluating MODIS soil fractional cover for arid
972 regions, using albedo from high-spatial resolution satellite imagery, Int. J. Remote Sens.,
973 35, 2028-2046, 2014.
- 974
- 975 [Le Quéré, C., Andrew, R. M., Canadell, J. G., Sitch, S., Korsbakken, J. I., Peters, G. P.,](#)
976 [Manning, A. C., Boden, T. A., Tans, P. P., Houghton, R. A., Keeling, R. F., Alin, S.,](#)
977 [Andrews, O. D., Anthoni, P., Barbero, L., Bopp, L., Chevallier, F., Chini, L. P., Ciais, P.,](#)
978 [Currie, K., Delire, C., Doney, S. C., Friedlingstein, P., Gkritzalis, T., Harris, I., Hauck, J.,](#)
979 [Haverd, V., Hoppema, M., Klein Goldewijk, K., Jain, A. K., Kato, E., Körtzinger, A.,](#)
980 [Landschützer, P., Lefèvre, N., Lenton, A., Lienert, S., Lombardozzi, D., Melton, J. R.,](#)
981 [Metzl, N., Millero, F., Monteiro, P. M. S., Munro, D. R., Nabel, J. E. M. S., Nakaoka, S.-](#)
982 [I., O'Brien, K., Olsen, A., Omar, A. M., Ono, T., Pierrot, D., Poulter, B., Rödenbeck, C.,](#)
983 [Salisbury, J., Schuster, U., Schwinger, J., Séférian, R., Skjelvan, I., Stocker, B. D.,](#)
984 [Sutton, A. J., Takahashi, T., Tian, H., Tilbrook, B., van der Laan-Luijkx, I. T., van der](#)
985 [Werf, G. R., Viovy, N., Walker, A. P., Wiltshire, A. J., and Zaehle, S.: Global Carbon](#)
986 [Budget 2016, Earth Syst. Sci. Data, 8, 605-649, doi:10.5194/essd-8-605-2016, 2016.](#)
- 987
- 988 Melton, J. R. and Arora, V. K.: Competition between plant functional types in the Canadian
989 Terrestrial Ecosystem Model (CTEM) v. 2.0, Geosci. Model Dev., 9, 323-361, 2016.

990
991 [Melton, J. R. and Arora, V. K. \(2014\) Sub-grid scale representation of vegetation in global land](#)
992 [surface schemes: Implications for estimation of the terrestrial carbon sink,](#)
993 [Biogeosciences, 11\(4\), 1021-1036.](#)
994
995 [Melton, J. R., Shrestha, R. K., and Arora, V. K.: The influence of soils on heterotrophic](#)
996 [respiration exerts a strong control on net ecosystem productivity in seasonally dry](#)
997 [Amazonian forests, Biogeosciences, 12, 1151-1168, doi:10.5194/bg-12-1151-2015, 2015.](#)
998
999 Peng, Y., Arora, V. K., Kurz, W. A., Hember, R. A., Hawkins, B. J., Fyfe, J. C., and Werner, A.
1000 T.: Climate and atmospheric drivers of historical terrestrial carbon uptake in the province
1001 of British Columbia, Canada, Biogeosciences, 11, 635-649, doi:10.5194/bg-11-635-2014,
1002 2014.
1003
1004 Pielke, R. A., Avissar, R., Raupach, M., Dolman, A. J., Zeng, X., and Denning, S.: Interactions
1005 between the atmosphere and terrestrial ecosystem: influence on weather and climate,
1006 Global Change Biology, 4, 461-475, 1998.
1007
1008 Ramankutty, N. and Foley, J. A.: Estimating historical changes in global land cover: Croplands
1009 from 1700 to 1992, Global Biogeochem. Cycles, 13, 997-1027, 1999.
1010
1011 Ran, L., Pleim, J., Gilliam, R., Binkowski, F. S., Hogrefe, C., and Band, L.: Improved
1012 meteorology from an updated WRF/CMAQ modeling system with MODIS vegetation
1013 and albedo, J. Geophys. Res. Atmos., 121, 2393-2415, doi:10.1002/2015JD024406, 2016.
1014
1015 [Ruesch, A. and Holly, K.: New IPCC Tier-1 Global Biomass Carbon Map For the Year 2000,](#)
1016 [available at: \[ftp://cdiac.ornl.gov/pub/global_carbon/\]\(ftp://cdiac.ornl.gov/pub/global_carbon/\) \(last access: 5 July 2013\), Carbon](#)
1017 [Dioxide Information Analysis Center <http://cdiac.ornl.gov> \(last access: 5 July 2013\), Oak](#)
1018 [Ridge National Laboratory, Oak Ridge, Tennessee, 2008.](#)
1019
1020 Ritchie, T. C. and Macdonald, G. M.: The patterns of post-glacial spread of White Spruce, J.
1021 Biogeogr., 13, 527-540, 1986.
1022
1023 Shrestha, R. K., Arora, V. K., and Melton, J. R.: The sensitivity of simulated competition
1024 between different plant functional types to sub-grid-scale representation of vegetation in
1025 a land surface model, J. Geophys. Res. Biogeosci., 121, doi:10.1002/2015JG003234,
1026 2016.
1027
1028 Siemann, E. and Rogers, W. E.: Changes in light and nitrogen availability under pioneer trees
1029 may indirectly facilitate tree invasion of grasslands, J. Ecology, 91, 923-931, 2003.
1030
1031 Sitch, S., Smith, B., Prentice, I. C., Arneeth, A., Bondeau, A., Cramer, W., Kaplan, J. O., Lucht,
1032 W., Sykes, M. T., Thonicke, K., and Venevsky, S.: Evaluation of ecosystem dynamics,
1033 plant geography and terrestrial carbon cycling in the LPJ dynamic global vegetation
1034 model, Glob. Change Biol., 9, 161-185, 2003.

1035 [Ste-Marie, C., Paré D. and Gagnon, D. : The contrasting effects of Aspen and Jack Pine on soil](#)
1036 [nutritional properties depend on parent material, *Ecosystems*, 10\(8\), 1299-1310, 2007.](#)
1037
1038 Teufel, B., Sushama, L., Arora, V., and Verseghy, D.: Impact of dynamic vegetation phenology
1039 on the simulated pan-Arctic land surface state, submitted to *Climate Dynamics*, 2017.
1040
1041 Timmons, D., Buchholz, T., and Veeneman, C. H.: Forest biomass energy: assessing
1042 atmospheric carbon impacts by discounting future carbon flows, *GCB Bioenergy*, 8, 631-
1043 643, 10.1111/gcbb.12276, 2016.
1044
1045 Verseghy, D. L., Mcfarlane, N. A., and Lazare, M.: CLASS - A Canadian land surface scheme
1046 for GCMs, II. Vegetation model and coupled runs, *Int. J. Climatol.*, 13, 347-370, 1993.
1047
1048 Viovy, N.: CRU-NCEP reanalysis data version 4. Available at
1049 [http://dods.extra.cea.fr/store/p529viouv/cruncep/V4_1901_2012/], (Accessed May 2015),
1050 2012.
1051
1052 Wang, A., Price, D. T., and Arora, V. K.: Estimating changes in global vegetation cover (1850-
1053 2100) for use in climate models, *Global Biogeochem. Cycles*, 20, GB3028, 2006.
1054
1055 Wang, G., Sun, S., and Mei, R.: Vegetation dynamics contributes to the multi-decadal variability
1056 of precipitation in the Amazon region, *Geophys. Res. Lett.*, 38, L19703,
1057 doi:10.1029/2011GL049017, 2011.
1058
1059 Wen, X., Tang, G., Wang, S., and Huang, J.: Comparison of global mean temperature series,
1060 *Advances in Climate Change Research*, 2, 187-192, 2011.
1061
1062 [Wu, Y., Verseghy, D. L. and Melton, J. R.: Integrating peatlands into the coupled Canadian Land](#)
1063 [Surface Scheme \(CLASS\) v3.6 and the Canadian Terrestrial Ecosystem Model \(CTEM\)](#)
1064 [v2.0, *Geosci Model Dev*, 9\(8\), 2639–2663, doi:10.5194/gmd-9-2639-2016, 2016.](#)
1065
1066 Zhang, Z., Xue, Y., Macdonald, G., Cox, P. M., and Collatz, G. J.: Investigation of North
1067 America vegetation variability under recent climate: A study using the
1068 SSiB4/TRIFFID biophysical/dynamic vegetation model, *J. Geophys. Res. Atmos.*, 120,
1069 1300-1321, 2015.
1070
1071 Zhu, Z., Bi, J., Pan, Y., Ganguly, S., Anav, A., Xu, L., Samanta, A., Piao, S., Nemani, R. R., and
1072 Myneni, R. B.: Global data sets of vegetation leaf area index (LAI)3g and fraction of
1073 photosynthetically active radiation (FPAR)3g derived from global inventory modeling
1074 and mapping studies (GIMMS) normalized difference vegetation index (NDVI)3g for the
1075 period 1981- to 2011, *Remote Sens.*, 5, 927-948, doi:10.3390/rs5020927, 2013.
1076
1077 Zobler, L.: A world soil file for global climate modelling, Tec. Rep. NASA TM-87802, 14-32,
1078 1986.
1079
1080

Formatted: English (U.S.)

Formatted: English (U.S.)

Formatted: English (U.S.)

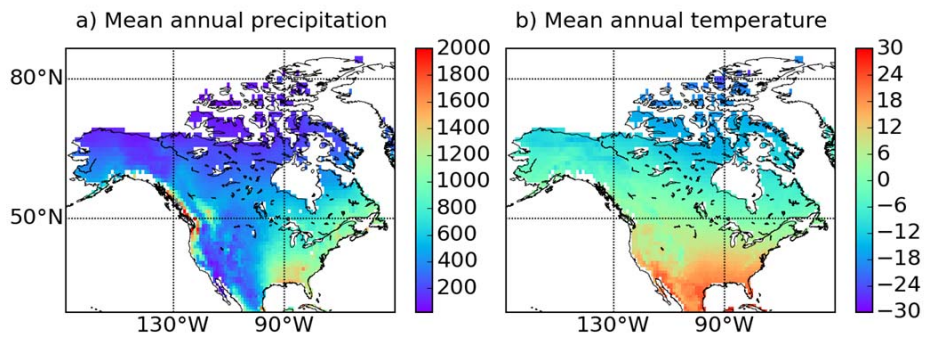
1081
 1082
 1083 Table 1: Plant functional types (PFTs) represented in CTEM and their relation to CLASS PFTs.
 1084
 1085

CLASS PFTs	CTEM PFTs	CTEM PFT Symbol
Needleleaf trees	Needleleaf Evergreen trees	NDL-EVG
	Needleleaf Deciduous trees	NDL-DCD
Broadleaf trees	Broadleaf Evergreen trees	BDL-EVG
	Broadleaf Cold Deciduous trees	BDL-DCD-CLD
	Broadleaf Drought/Dry Deciduous trees	BDL-DCD-DRY
Crops	C ₃ Crops	CROP-C3
	C ₄ Crops	CROP-C4
Grasses	C ₃ Grasses	GRASS-C3
	C ₄ Grasses	GRASS-C4

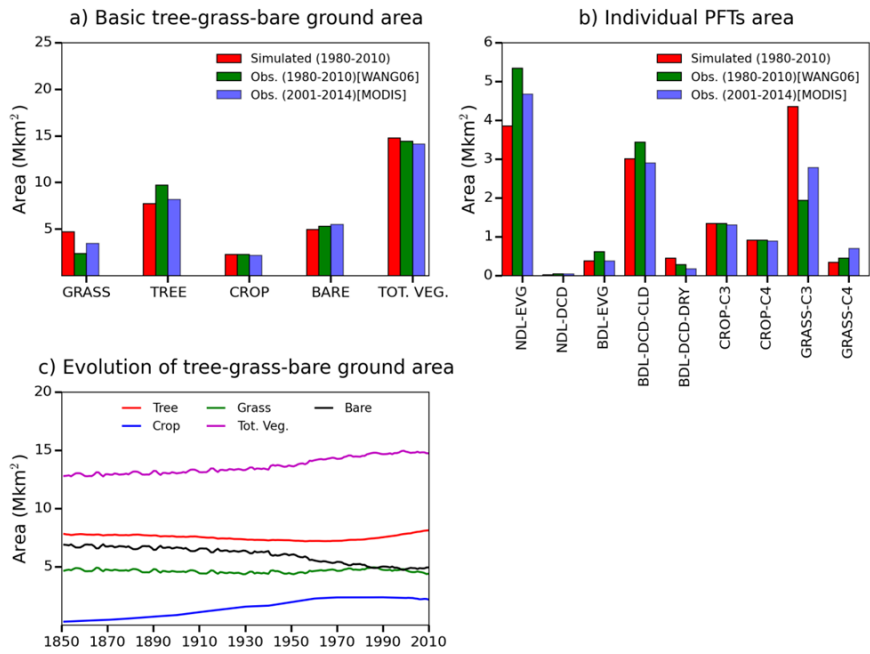
Table 2: Reclassification of the 17 MODIS land cover classes into the nine CTEM PFTs

SN	Items	Tree				Crop	Grass	Bare	Reference
		NDL EVG	NDL DCD	BDL EVG	BDL DCD				
1	Woody Savanna			0.1	0.4		0.25	0.25	Dai et al. (2001)
2	Water bodies							1	
3	Urban built up areas	0.05			0.05		0.1	0.8	Dai et al. (2001)
4	Savanna			0.05	0.3		0.4	0.25	Wang et al. (2006)
5	Permanent Wetlands						0.25	0.75	Dai et al. (2001)
6	Permanent snow and ice							1	Wang et al. (2006)
7	Open Shrublands	0.1			0.15		0.35	0.4	Wang et al. (2006)
8	Needleleaf evergreen	1							Wang et al. (2006)
9	Needleleaf deciduous		0.8				0.1	0.1	Wang et al. (2006)
10	Mixed forest	0.45			0.45		0.1		Wang et al. (2006)
11	Grasslands						0.65	0.35	Wang et al. (2006)
12	Croplands					0.9		0.1	Wang et al. (2006)
13	Cropland natural veg. mosaic			0.2		0.5	0.2	0.1	Wang et al. (2006)
14	Closed shrublands	0.2	0.2		0.4		0.2		Wang et al. (2006)
15	Broadleaf evergreen			1					Wang et al. (2006)
16	Broadleaf deciduous				1				Wang et al. (2006)
17	Bare ground							1	Wang et al. (2006)

1
2
3



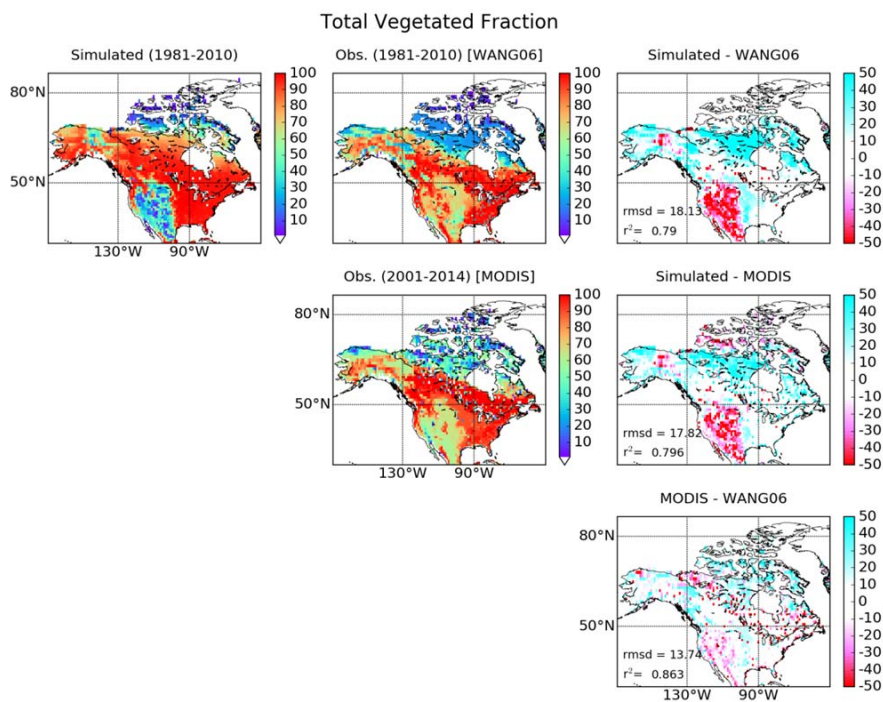
4
5 Figure 1. Spatial distribution of mean annual a) precipitation (mm), and b) temperature (°C)
6 across North America. Grid cells with permanent ice/glaciers have been masked out.
7



8

9

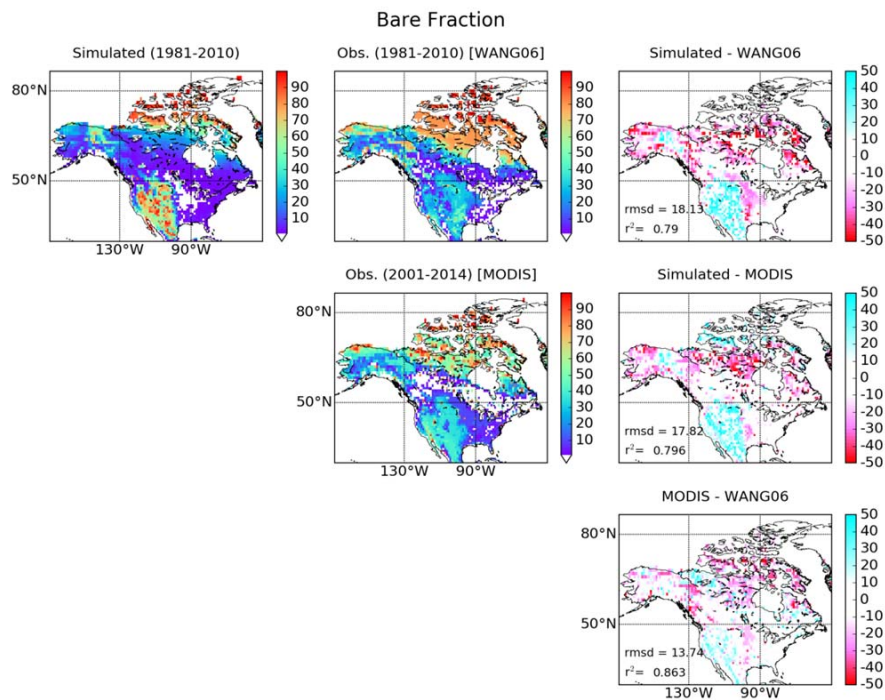
10 Figure 2. Comparison of observation-based and simulated vegetation areas summed over the
 11 North American domain a) grass, treed, crop, bare ground and total vegetated area, b) individual
 12 PFT areas, and c) evolution of simulated vegetation areas summed over the domain.
 13



15

16 Figure 3. Spatial distribution of total vegetated coverage across North America. Simulated,
 17 observation-based, and differences are presented in the left, middle and right columns,
 18 respectively. The differences column includes model biases with respect to WANG06 (top panel)
 19 and MODIS (middle panel), and the difference between the two observation-based estimates
 20 (bottom panel). Root mean square difference (rmsd) and coefficient of determination (r^2) are also
 21 shown in each case.

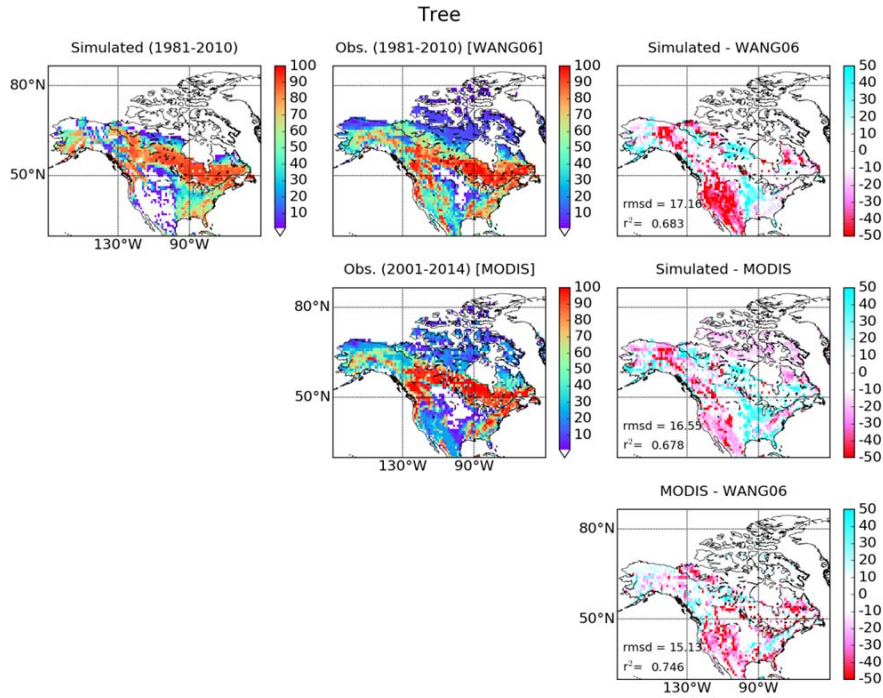
22



24
 25 Figure 4. Spatial distribution of bare ground coverage across North America. Simulated,
 26 observation-based, and differences are presented in the left, middle and right columns,
 27 respectively. The differences column includes model biases with respect to WANG06 (top panel)
 28 and MODIS (middle panel), and the difference between the two observation-based estimates
 29 (bottom panel). Root mean square difference (rmsd) and coefficient of determination (r^2) are also
 30 shown in each case.

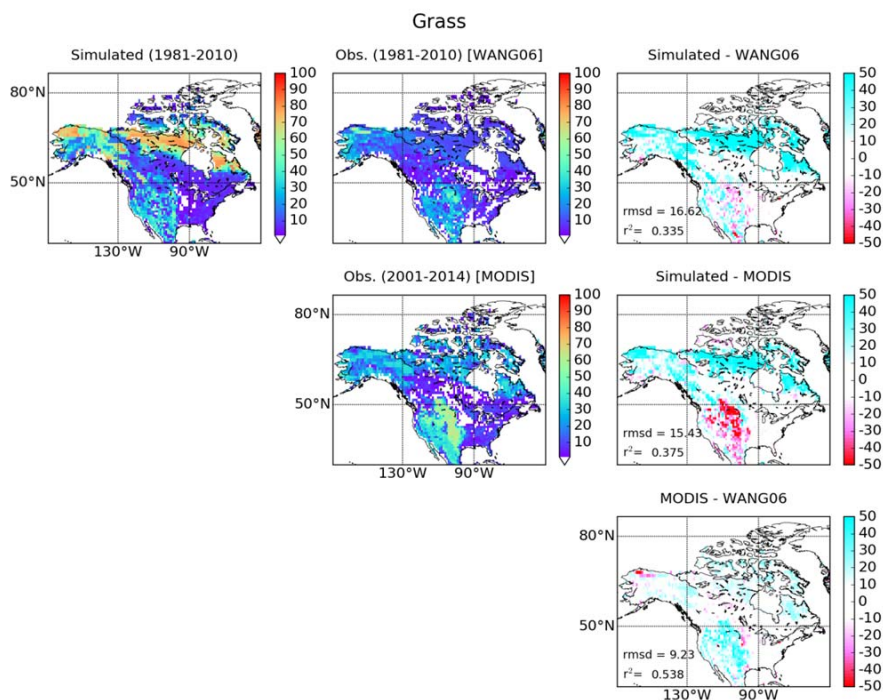
31

32



33
 34 Figure 5. Spatial distribution of tree coverage across North America. Simulated, observation-
 35 based, and differences are presented in the left, middle and right columns, respectively. The
 36 differences column includes model biases with respect to WANG06 (top panel) and MODIS
 37 (middle panel), and the difference between the two observation-based estimates (bottom panel).
 38 Root mean square difference (rmsd) and coefficient of determination (r^2) are also shown in each
 39 case.

40



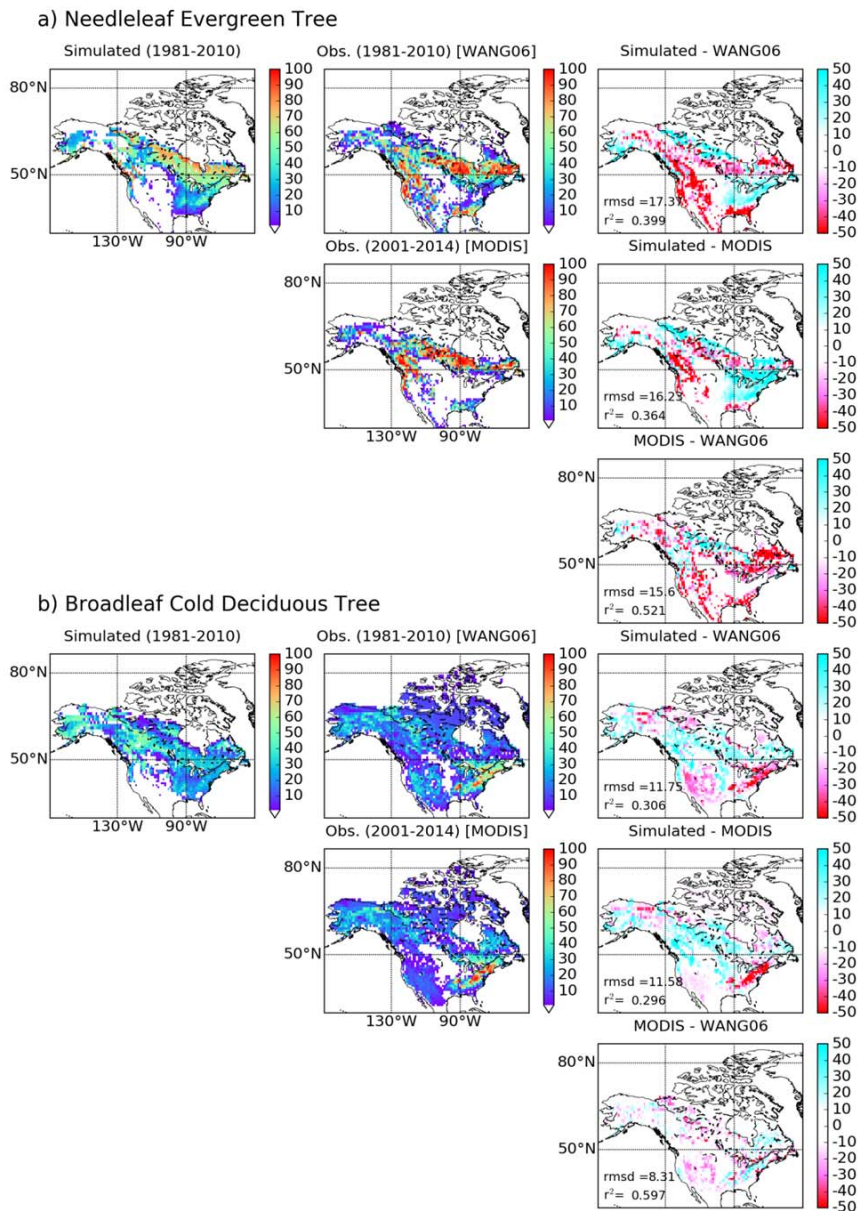
42

43 Figure 6. Spatial distribution of grass coverage across North America. Simulated, observation-
 44 based, and differences are presented in the left, middle and right columns, respectively. The
 45 differences column includes model biases with respect to WANG06 (top panel) and MODIS
 46 (middle panel), and the difference between the two observation-based estimates (bottom panel).
 47 Root mean square difference (rmsd) and coefficient of determination (r^2) are also shown in each
 48 case.

49

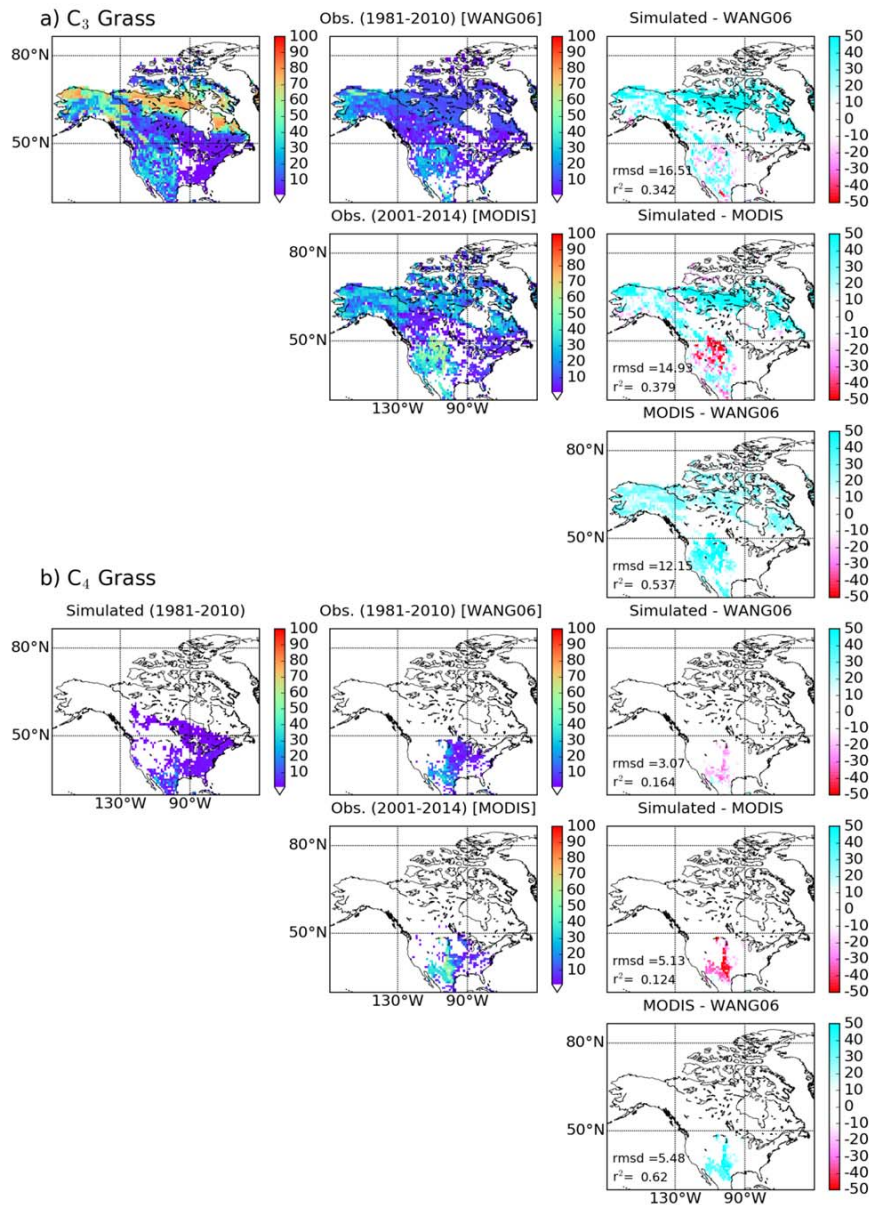
50

51



52

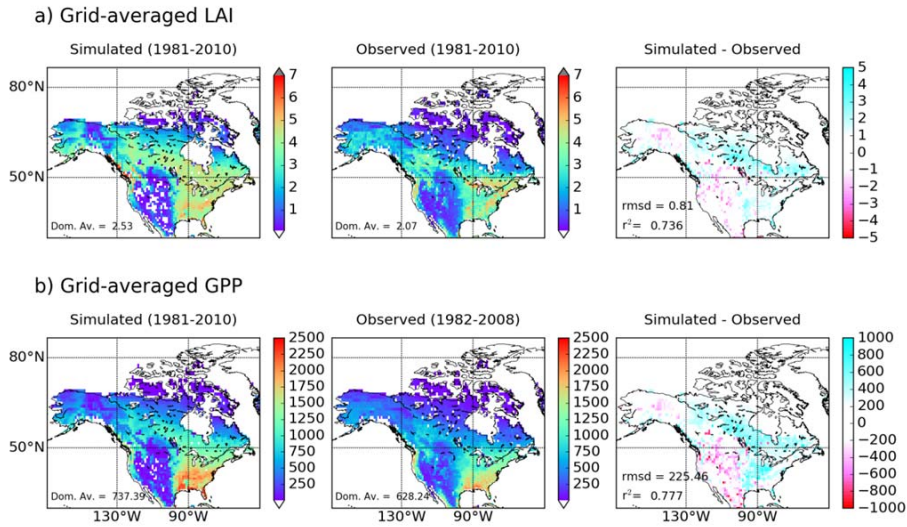
53 Figure 7. Spatial distribution of a) needleleaf evergreen tree, and b) broadleaf cold deciduous tree
 54 across North America. Simulated, observation-based, and differences are presented in the left,
 55 middle and right columns, respectively. The differences column includes model biases with
 56 respect to WANG06 (top panel) and MODIS (middle panel), and the difference between the
 57 observation-based estimates (bottom panel). Root mean square difference (rmsd) and coefficient
 58 of determination (r^2) are also shown in each case.



59

60 Figure 8. Spatial distribution of a) C₃ grasses, and b) C₄ grasses across North America.
 61 Simulated, observation-based, and differences are presented in the left, middle and right
 62 columns, respectively. The differences column includes model biases with respect to WANG06
 63 (top panel) and MODIS (middle panel), and the difference between the the observation-based
 64 estimates (bottom panel). Root mean square difference (rmsd) and coefficient of determination
 65 (r²) are also shown in each case.

66
67
68
69



70
71
72
73
74
75
76

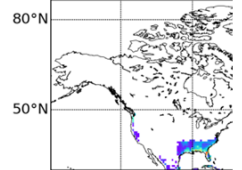
Figure 9. Spatial distribution of a) grid averaged maximum LAI ($m^2 m^{-2}$), and b) grid averaged GPP ($g C m^2 y^{-1}$) across North America. Simulated, observation-based, and differences between them are presented in the left, middle and right columns, respectively. Root mean square difference (rmsd) and coefficient of determination (r^2) are also shown in each case.

Deleted: ¶

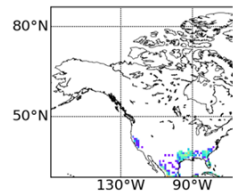
¶

a) Broadleaf Evergre

Simulated (1981-2010)



b) Broadleaf Dry De



¶
Figure 9. Spatial distribution of a) broadleaf evergreen tree, and b) broadleaf dry deciduous tree across North America. Simulated, WANG06 and MODIS distribution are presented in the left, middle and right columns, respectively. ¶

¶

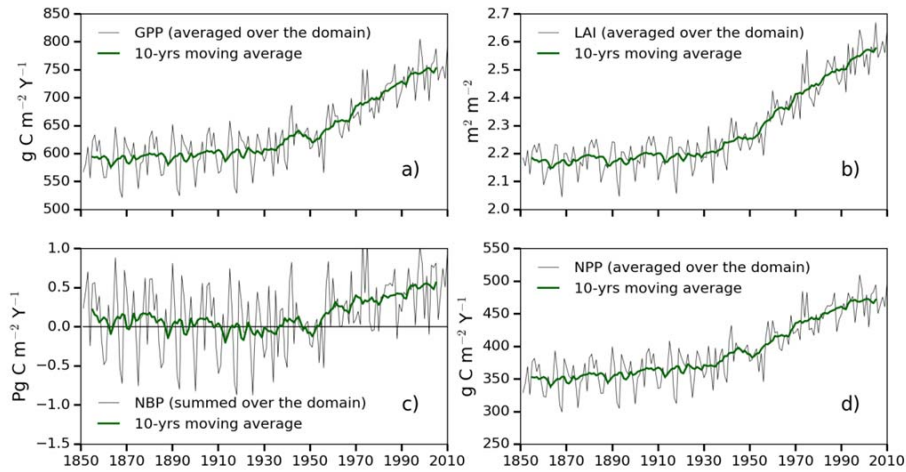
¶

¶

-----Page Break-----

Deleted: 10

94



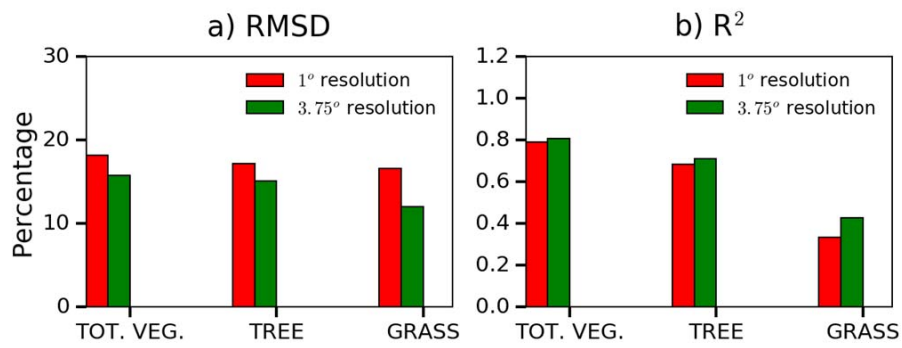
95

96

97 | Figure 10. Time series evolution of a) domain averaged GPP ($\text{g C m}^{-2} \text{y}^{-1}$), b) domain averaged
98 | LAI ($\text{m}^2 \text{m}^{-2}$), c) domain total NBP ($\text{Pg C m}^{-2} \text{y}^{-1}$), and d) domain averaged NPP ($\text{g C m}^{-2} \text{y}^{-1}$).

99 |

100
101
102

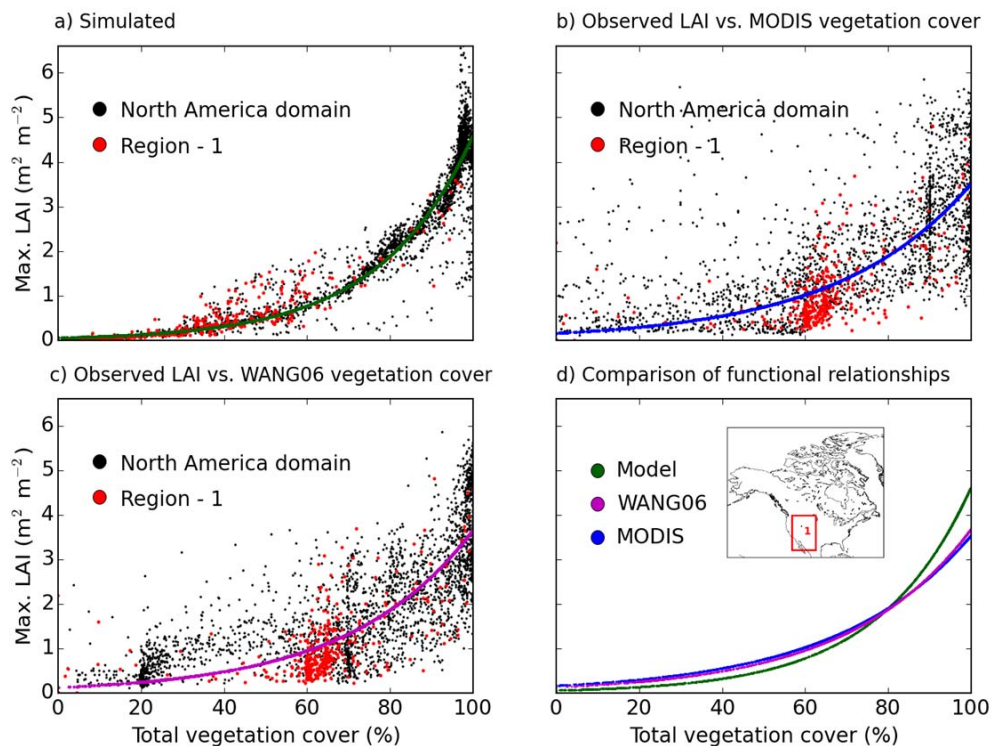


103
104
105
106
107
108
109
110
111

Figure 11. Comparison of the performance of the model at the 1° spatial resolution in this study with that at the 3.75° spatial resolution in the Melton and Arora (2016) study. The Melton and Arora (2016) global results were extracted for the North American domain. Spatial correlations and root mean square differences are used as metrics for the comparison between simulated and the observation-based estimate based on the modified WANG06 land cover product for fractional coverage of total vegetation, tree and grass.

112

113



114

115

116 Figure 12. Scatter plots of a) simulated LAI vs. simulated total vegetation coverage, b) observed
117 LAI vs. MODIS-derived total vegetation coverage, c) observed LAI vs. WANG06 total
118 vegetation coverage. Plot d) shows a comparison of the fitted curves represented by solid lines,
119 with an inset map of North America showing the sub-domain of interest bounded by a red
120 rectangle.

121

122